NASA/TM–2009-215380

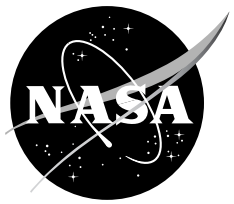

JVX Proprotor Performance Calculations and Comparisons with Hover and Airplane-Mode Test Data

C. W. Acree, Jr.
Ames Research Center, Moffett Field, California

April 2009

The NASA STI Program Office . . . in Profile

Since its founding, NASA has been dedicated to the advancement of aeronautics and space science. The NASA Scientific and Technical Information (STI) Program Office plays a key part in helping NASA maintain this important role.

The NASA STI Program Office is operated by Langley Research Center, the Lead Center for NASA's scientific and technical information. The NASA STI Program Office provides access to the NASA STI Database, the largest collection of aeronautical and space science STI in the world. The Program Office is also NASA's institutional mechanism for disseminating the results of its research and development activities. These results are published by NASA in the NASA STI Report Series, which includes the following report types:

- TECHNICAL PUBLICATION. Reports of completed research or a major significant phase of research that present the results of NASA programs and include extensive data or theoretical analysis. Includes compilations of significant scientific and technical data and information deemed to be of continuing reference value. NASA's counterpart of peer-reviewed formal professional papers but has less stringent limitations on manuscript length and extent of graphic presentations.

- TECHNICAL MEMORANDUM. Scientific and technical findings that are preliminary or of specialized interest, e.g., quick release reports, working papers, and bibliographies that contain minimal annotation. Does not contain extensive analysis.

- CONTRACTOR REPORT. Scientific and technical findings by NASA-sponsored contractors and grantees.

- CONFERENCE PUBLICATION. Collected papers from scientific and technical conferences, symposia, seminars, or other meetings sponsored or cosponsored by NASA.

- SPECIAL PUBLICATION. Scientific, technical, or historical information from NASA programs, projects, and missions, often concerned with subjects having substantial public interest.

- TECHNICAL TRANSLATION. English-language translations of foreign scientific and technical material pertinent to NASA's mission.

Specialized services that complement the STI Program Office's diverse offerings include creating custom thesauri, building customized databases, organizing and publishing research results . . . even providing videos.

For more information about the NASA STI Program Office, see the following:

- Access the NASA STI Program Home Page at *http://www.sti.nasa.gov*

- E-mail your question via the Internet to help@sti.nasa.gov

- Fax your question to the NASA Access Help Desk at (301) 621-0134

- Telephone the NASA Access Help Desk at (301) 621-0390

- Write to:
  NASA Access Help Desk
  NASA Center for AeroSpace Information
  7115 Standard Drive
  Hanover, MD 21076-1320

NASA/TM–2009-215380

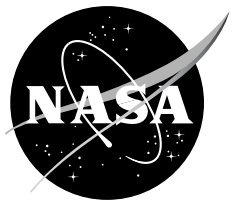

JVX Proprotor Performance Calculations and Comparisons with Hover and Airplane-Mode Test Data

C. W. Acree, Jr.
Ames Research Center, Moffett Field, California

National Aeronautics and
Space Administration

Ames Research Center
Moffett Field, California 94035-1000

April 2009

Acknowledgments

The author wishes to express his appreciation to Randy Peterson for providing the JVX Phase II airplane-mode data, and to Wayne Johnson for his assistance in planning and conducting the research.

Available from:

NASA Center for AeroSpace Information
7115 Standard Drive
Hanover, MD 21076-1320
(301) 621-0390

National Technical Information Service
5285 Port Royal Road
Springfield, VA 22161
(703) 487-4650

TABLE OF CONTENTS

LIST OF FIGURES

LIST OF TABLES

NOTATION

CFD	computational fluid dynamics
CSD	computational structural dynamics
DNW	Deutsch-Niederlandischer Windkanal
JVX	Joint Vertical Experimental
LCTR	Large Civil Tiltrotor
NFAC	National Full-Scale Aerodynamics Complex
OARF	Outdoor Aerodynamic Research Facility
PTR	Propeller Test Rig
RDRS	Rotor Data Reduction System
TRAM	Tilt Rotor Aeroacoustic Model
VTOL	vertical takeoff and landing

A	rotor disk area
K_L	stall-delay factor for lift (Corrigan model)
K_{sdD}	stall-delay factor for drag (Selig model)
K_{sdL}	stall-delay factor for lift (Selig model)
c	blade chord
c_d	airfoil-section drag coefficient
c_{d_L}	linear approximation of drag coefficient
$c_{d\text{table}}$	drag coefficient from airfoil table
c_{dz}	drag coefficient at zero lift
c_l	airfoil-section lift coefficient
c_{l_L}	linear extension of c_l vs. α curve
$c_{l\text{table}}$	lift coefficient from airfoil table
$c_{l\alpha}$	lift-curve slope
C_P	rotor power coefficient, $P/(\rho A V_{tip}^3)$
C_{Pi}	induced power coefficient, $P_i/(\rho A V_{tip}^3)$
$C_{P\text{ideal}}$	ideal power coefficient, $C_T^{3/2}/\sqrt{2}$
C_{Po}	profile power coefficient, $P_o/(\rho A V_{tip}^3)$
C_T	rotor thrust coefficient, $T/(\rho A V_{tip}^2)$
D	exponent in stall-delay factor
FM	rotor hover figure of merit, $\left(T\sqrt{T/2\rho A}\right)/P$
M_{tip}	rotor-tip Mach number
n	exponent in Reynolds number correction
P	rotor power
P_i	rotor induced power
P_o	rotor profile power
r	local blade radius
R	rotor radius
Re	Reynolds number
Re_t	reference Reynolds number
T	rotor thrust
V	flight speed (rotor axial velocity)
V_{tip}	rotor tip speed
V_{tun}	wind tunnel airspeed
α	angle of attack
α_z	zero-lift angle of attack
η	propulsive efficiency, TV/P
Γ	blade-section circulation
κ	induced power ratio, $C_{Pi}/C_{P\text{ideal}}$
κ_λ	factor on induced velocity
μ	advance ratio, V/V_{tip}
Ω	rotor rotational speed
ρ	air density
σ	rotor solidity (ratio blade area to disk area)

JVX PROPROTOR PERFORMANCE CALCULATIONS AND COMPARISONS WITH HOVER AND AIRPLANE-MODE TEST DATA

C. W. Acree, Jr.

Ames Research Center

ABSTRACT

A 0.656-scale V-22 proprotor, the Joint Vertical Experimental (JVX) rotor, was tested at the NASA Ames Research Center in both hover and airplane-mode (high-speed axial flow) flight conditions, up to an advance ratio of 0.562 (231 knots). The hover and airplane-mode data were used to develop improved proprotor aerodynamic models. A new, multiple-trailer free-wake model is shown to give improved predictions of hover performance while also providing good predictions of airplane-mode performance. Predictions with simpler aerodynamic models are also included, along with discussions of stall-delay models and comparisons with Tilt Rotor Aeroacoustic Model (TRAM) hover data.

INTRODUCTION

The research reported here was initiated as part of efforts to exploit and extend the results of the NASA Heavy Lift Rotorcraft Systems Investigation (ref. 1). That effort was directed towards the short-haul civil market, with ambitious efficiency, noise, and cost requirements deliberately chosen to stimulate advanced vertical takeoff and landing (VTOL) technology development. The Large Civil Tiltrotor (LCTR) was selected as having the best potential of several configurations to meet NASA technology goals.

With the LCTR selected as the preferred design, research turned towards increasingly sophisticated proprotor designs. This focus motivated a reexamination of the analytical tools used to predict rotor performance and the test data used to validate the methodology. The intent was to improve both the accuracy and efficiency of rotor performance predictions, including quantifying the trade-offs between computational speed and numerical accuracy. The emphasis was on proprotors, with higher twist and lower aspect ratio than conventional helicopter rotors. Whether improved in accuracy or simplified for efficiency, the analytical methods required validation against test data.

The JVX rotor was an experimental precursor to the V-22 rotor, hence the name "Joint Vertical Experimental." Sometimes referred to as a "2/3-scale V-22," it in fact differed from the V-22 in several respects, as described in a later section, "The JVX Test Rotor." Complete JVX hover test data were published in reference 2, and very limited airplane-mode data from a subsequent 40- by 80-foot wind tunnel test were published in reference 3. A much more extensive set of airplane-mode wind tunnel data acquired in 1991 is published herein. Both the hover and airplane-mode JVX data are compared with predictions having several levels of sophistication. Limited comparisons with 1/4-scale V-22 data (the Tilt Rotor Aeroacoustic Model, or TRAM) are also included.

This report is an expanded version of a paper originally published as reference 4, and includes two new appendices with tabulated test data and the CAMRAD II rotor model.

This report begins with a description of the JVX rotor and test history, plus a brief description of the TRAM rotor. The predictive methodology is then described, including two different free-wake models and two stall-delay models; Reynolds number corrections are also summarized. Comparison of hover performance predictions to test data then follows, including brief descriptions of additional inflow models: uniform inflow, differential momentum, and prescribed wake. The report concludes with comparison of airplane-mode predictions to test data.

DESCRIPTION OF EXPERIMENTS

The JVX rotor has spawned several progeny, each with slightly different characteristics. JVX hover performance was better than expected because of three-dimensional (3-D) rotational stall-delay effects, which were not well understood at the time. The full-scale V-22 was subse-

quently built with slightly lower solidity than JVX and with a blade-fold hinge and fairing. The BA 609 rotor is similar to JVX, although slightly larger in diameter and with a different root airfoil section (ref. 5). It also has lower solidity than the JVX rotor. The BA 609 rotor is not, therefore, identical to either JVX or V-22. Several small-scale aircraft, such as the Eagle Eye, also use aerodynamically similar rotors. None of these rotors is an exact scaled version of another, and their differences, although sometimes small, must be kept in mind when comparing performance data.

The JVX Test Rotor

The JVX rotor was tested in two different aerodynamic configurations, so care must be taken when comparing it to the production V-22 rotor and other scaled V-22 rotors, such as the TRAM, described in the next section. The following description includes information from references 2 and 3. See also reference 6 for JVX airfoil data.

The JVX rotor was built by Bell-Boeing and tested at NASA Ames Research Center. The rotor was 25 feet in diameter, which is 0.656 scale relative to the as-built V-22 design. In addition to scale, the JVX model and the V-22 had other differences. The JVX rotor used an XV-15 hub with fixed, 2.5-deg precone, whereas the V-22 hub has a coning flexure with slightly different at-rest precone. An XV-15 spinner was used for the JVX, instead of the much shorter V-22 spinner. The JVX rotor-blade configuration differed from the V-22 in taper, twist, and airfoil distribution, with linear taper and an XN-28 airfoil at the root. JVX solidity was 8% greater than the V-22, as described in reference 7.

The diameter of the V-22 rotor was slightly enlarged for production. The JVX test rotor is 0.658 scale referred to the original V-22 diameter. This slightly larger scale value is sometimes encountered in the literature (e.g., ref. 2) and does not imply any changes to the JVX test article.

JVX airplane-mode testing was done with a thicker root section that modeled the V-22 production blade, which has a thick root to accommodate a folding hinge. The JVX rotor was tested on the Propeller Test Rig (PTR), which has a fairing over the rotor balance just behind the hub. The trailing edges at the blade roots were slightly clipped to clear the rotor balance fairing (figs. 1 and 2). These differences at the blade root are the reasons for the differences in taper, twist, and airfoil distribution between JVX and V-22. The difference in solidity results from a proportional adjustment to chord (ref. 7).

Figure 1. The JVX rotor mounted on the PTR for hover tests at the OARF (1984).

Figure 2. The JVX rotor mounted on the PTR for airplane-mode tests in the NFAC 40- by 80-ft test section (1991).

The TRAM Test Rotor

The TRAM is a 1/4-scale V-22, designed for acoustics and blade loads measurements (ref. 8). It was tested as both a full-span model with two rotors and as an isolated rotor. Figure 3 shows the TRAM isolated-rotor configuration, as installed in the Deutsch-Niederlandischer Windkanal (DNW) for airplane-mode tests.

The JVX and TRAM rotor characteristics are summarized in table 1, with V-22 data for reference. The test conditions for data presented in this report are summarized in table 2. Additional details are given in reference 9, from which tables 1 and 2 have been redacted.

JVX AND TRAM ROTOR TESTS

JVX hover tests were performed at the Outdoor Aerodynamic Research Facility (OARF) at NASA Ames Research Center in 1984 (ref. 2). The hover data presented in this report are tabulated in appendix A and are a subset of those in reference 2.

Figure 3. TRAM isolated rotor in airplane-mode configuration in the DNW (1998).

The hover tests on the OARF (fig. 1) were free from recirculation effects and most wall interference effects (excepting the ground, as can be seen in fig. 1). The test data presented herein were all taken near dawn, at very low wind conditions. Although some tests were conducted with a scaled V-22 wing installed to measure download, all data shown were taken without the wing and were selected for minimum wind (less than 1 knot).

High-speed (airplane mode) and wing download and interference tests were conducted in the 40- by 80-ft test section of the NFAC at NASA Ames, divided into three test phases. Phase I tests were conducted in 1988, for which only very limited airplane-mode data were collected and published (ref. 3). Phase II airplane-mode tests were subsequently conducted in 1991 in the NFAC 40- by 80-ft test section. Phase II performance data used in the present report are tabulated in appendix A. Phase III was intended to complete the airplane-mode dataset, but the rotor was destroyed in an accident very early in the test.

The airplane-mode data presented here are all from the Phase II test (fig. 2). Although the maximum speed attained was below the desired goal of 300 knots, the data are adequate to validate analyses used for design optimization.

Some JVX airplane-mode tests were conducted with a wing or with the PTR yawed with respect to the flow, but all data shown were taken without the wing and at zero yaw angle. Standard test procedure was to set the rotor rpm and tunnel airspeed, and then vary collective to vary thrust and power at a fixed advance ratio. The data presented cover five distinct advance ratios. The criteria for data selection were no wing, no yaw angle, and enough data points at each advance ratio for meaningful comparisons with predictions.

The TRAM was tested as an isolated rotor in the DNW in 1988 (ref. 10). The data presented here are a subset of those in reference 10. During the DNW tests, TRAM was operated up to 89% design rotor speed in hover. TRAM hover data presented in this report are limited to this high-power condition in order to best match the JVX test conditions. TRAM airplane mode tests were conducted over a limited range of advance ratios; the resulting performance data are presented herein.

TABLE 1. JVX AND TRAM ROTOR CHARACTERISTICS

	JVX	TRAM	V-22
Scale, referenced to V-22	0.656	0.25	1
Rotor radius (in.)	150	57	228.5
Solidity (thrust weighted)	0.1138	0.105	0.105
Tip chord (in.)	15.79	5.5	22.0
Taper (tip/root chord)	0.65	0.62	0.637

TABLE 2. JVX AND TRAM SUMMARY TEST CONDITIONS

	JVX hover	JVX airplane mode	TRAM hover	TRAM airplane mode
Tip Mach no.	0.676	0.575, 0.625	0.628	0.593
Tip speed (ft/sec)	754	640, 695	701	662
Airspeed (knots)	0	100–231	0	127–147

Data from several hover tests of V-22 scale models are compared to the V-22 flight data in reference 11, whereas only the JVX and TRAM DNW tests provide data for an isolated rotor. While the TRAM rotor has a hub more representative of the V-22, its blade root is not an exact match to the V-22. Moreover, the DNW tests of TRAM have greater flow blockage than the PTR. The TRAM nacelle is 1/4-scale V-22, but not the model support mechanism, which is relatively large, as can be seen in figure 3. Thus, even discounting scale effects, cross-correlation between isolated-rotor datasets is limited and somewhat compromised.

For this report, JVX rotor data are emphasized over TRAM data because of the larger scale, the wider range of airplane-mode data, and the inherently greater accuracy of the PTR for performance measurements. Because the larger purpose of the present research is to develop improved analytical techniques, quality of the data is considered more important than an exact match to the actual V-22.

THEORETICAL ANALYSES

The rotor performance code used here is CAMRAD II (ref. 12), a comprehensive rotorcraft analysis code with a free-wake model, a multi-element structural-beam model, and a choice of stall-delay models. The blade-element aerodynamic model relies upon 2-D airfoil tables and adds corrections for yawed flow, Reynolds number, 3-D stall delay, and other effects. CAMRAD II is much more computationally efficient than any comparable computational fluid dynamics/computational structural dynamics CFD/CSD) code. The version (Release 4.6) used for this study has a revised free-wake model that includes an improved wake-distortion integration algorithm.

For this report, five different levels of aerodynamic modeling were evaluated: uniform inflow, differential momentum (the CAMRAD II implementation of combined blade-element/momentum theory), prescribed wake (based on the Kocurek and Tangler model), rolled-up free wake, and multiple-trailer free wake. The CAMRAD II wake models have been thoroughly documented elsewhere, notably reference 13, and are summarized in the following section, with emphasis on the differences between the rolled-up and multiple-trailer models. The simpler models—uniform inflow, differential momentum, and prescribed wake—rely upon empirical adjustments and are accordingly discussed in the context of the experimental data.

Two 3-D stall-delay models were also evaluated. They are discussed in detail in a separate section, "Stall-Delay Models." The effects of Reynolds number corrections were also evaluated.

All analyses reported here used modeling options built into CAMRAD II. Appendix B gives CAMRAD II inputs for the rotor, wake, and stall-delay models.

Wake Models

Unless otherwise noted, predictions of JVX hover performance presented in this report were made with the default CAMRAD II free-wake model, with a strong vortex at the tip, a weak vortex at the root, and a vortex

sheet in between. The shed vorticity is eventually rolled up into a single tip vortex (the rolled-up model). Predictions were also made with a multiple-trailer model, having an additional vortex trailer slightly inboard of the radius at which blade-vortex interaction is experienced in hover. The multiple-trailer model used in this research is a simplified version of the one developed for the TRAM in airplane mode (ref. 10).

Some insight into the need for a multiple-trailer wake can be gained from a plot of circulation versus radius for different thrust levels (fig. 4), here calculated for the JVX rotor using the rolled-up wake model. At low thrust, blade-vortex interaction is seen slightly outboard of 90% radius. This result is consistent with the results reported for the TRAM in reference 9.

At high thrust, the rapid decrease in circulation near the tip results in a strong tip vortex. In the CAMRAD II rolled-up model, the strength of the tip vortex is determined from the peak bound circulation. Over the working portion of the blade (about 25–90% radius), circulation varies much more slowly, and the trailed vorticity is modeled with a vortex sheet, which is rolled up into the tip vortex. At low thrust, however, this model breaks down: circulation decreases rapidly enough from 30% to 80% radius that the tip-vortex roll-up model is inadequate. At extremely low thrust, the angle of attack near the tip is negative, as are the circulation and the sign of the tip vortex. Thus a conventional tip-vortex model is invalid for highly twisted blades at low thrust.

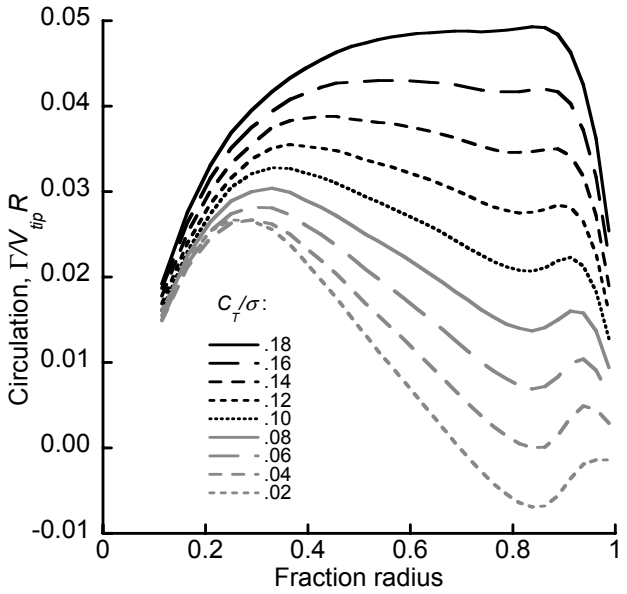

Figure 4. Predicted effect of JVX hover thrust on radial distribution of circulation.

This problem is addressed here by adding a vortex trailer at 80% radius. CAMRAD II automatically determines the appropriate sign and strength of each trailer (80% radius and tip), based upon the circulation inboard of each trailer. In this model, the two trailers are independent and never combine into a single tip vortex.

The multiple-trailer model used here is distinct from the CAMRAD II "dual-peak" wake model. The latter is intended for use with negative tip loading, whereas the former applies to both positive and negative tip loading.

Although the multiple-trailer model can significantly improve accuracy, there is a considerable cost in computational time (up to an order of magnitude greater). Moreover, convergence is poor at low thrust. Convergence problems and computational time are closely related: methods of improving convergence include reducing trim-loop relaxation factors, adding more wake iterations and sub-iterations, tightening tolerances on loop convergence, etc.—all of which increase computational time. These computational problems reflect a fundamental difficulty: the physical wake is unstable and chaotic, so the more accurately it is modeled, the more inefficient the solution procedure becomes.

The most effective means of improving convergence of the multiple-trailer model was to specify the growth rate of the inboard vortex core. A square-law growth rate was used, for which the core grew from 0.2 mean chord at the blade to 1.0 chord after five rotor revolutions. All predictions shown here for the multiple-trailer wake used this core-growth model. Core growth was not required to achieve convergence of the rolled-up model.

One objective of this investigation is to develop methods of analysis that can be used for design optimization. Therefore, a computationally efficient model is imperative. Rotors are optimized for high thrust in hover, so the CAMRAD II rolled-up wake model is adequate in most cases. An example is calculation of the effects of 3-D stall delay, which are seen primarily at high thrust, where the rolled-up model is adequate.

A more elaborate multiple-trailer model also available in CAMRAD II allows up to one trailer per aerodynamic panel, with an option to consolidate the trailers in the far wake (ref. 10). That model, however, was developed for loads predictions in edgewise flight and has not been validated against hover data. Moreover, computational requirements for that model are exorbitant, at least for design optimization. Research on more complex models continues, but the rolled-up wake model is currently pre-

ferred for design optimization, and the model with one additional trailer is sufficient where increased accuracy is needed at low thrust.

Stall-Delay Models

Proprotors are known to generate much more lift inboard than would be predicted from 2-D airfoil section data alone. The rotating blade experiences centrifugal pumping of the airflow, which accelerates the boundary layer and greatly delays stall. The effect is strongest at the root. CAMRAD II provides options to account for this effect, including two different methods of correcting 2-D airfoil data to compensate for 3-D stall delay.

The two stall-delay models are the Corrigan and Selig models, derived from references 14 and 15, respectively. Examples of adjustments to 2-D properties for the familiar NACA 0012 airfoil are given in figure 5, and examples of radial distributions for the JVX rotor are given in figure 6. At angles of attack greater than 30 deg, the stall-delay corrections are washed out so that the uncorrected airfoil properties are used in the post-stall region.

Both models include empirical adjustments. The values used for the present study are derived from references 14 and 15 and are given in the figures and equations in this section.

In CAMRAD II, the variation of stall delay with radius or airfoil is specified separately from the choice of model. Although it complicates the input, specification of radial variation independently of the model provides for maximum flexibility in accommodating different rotor designs and stall-delay models. For the present study, the section corrections and radial distributions were matched to each other in accordance with the models in references 14 and 15.

The Corrigan model shifts the peak lift and stall recovery portion of the curve upwards along a line defined by the lift curve slope at zero c_l, linearly extrapolated well beyond the normal stall angle (fig. 5). The extrapolated, linear lift curve is labeled "extended c_l" in the figure. In contrast, the Selig model (ref. 15) is a weighted interpolation between the extended c_l and the airfoil table c_l, with a similar correction for c_d. In CAMRAD II, α, c_l, and c_d may be further modified to account for blade sweep, yawed flow, Reynolds number, and other aerodynamic effects.

Figure 6 shows the variations of stall-delay factors with radius for the JVX rotor (OARF configuration). The Selig corrections are applied to lift and drag, with factors K_{sdL} and K_{sdD}, respectively; the Corrigan model applies only to lift. The Selig model is nonmonotonic with radius, so for the CAMRAD II JVX model, the Selig stall-delay factors are set to their maximum values at extreme inboard radii (the dashed lines in fig. 6).

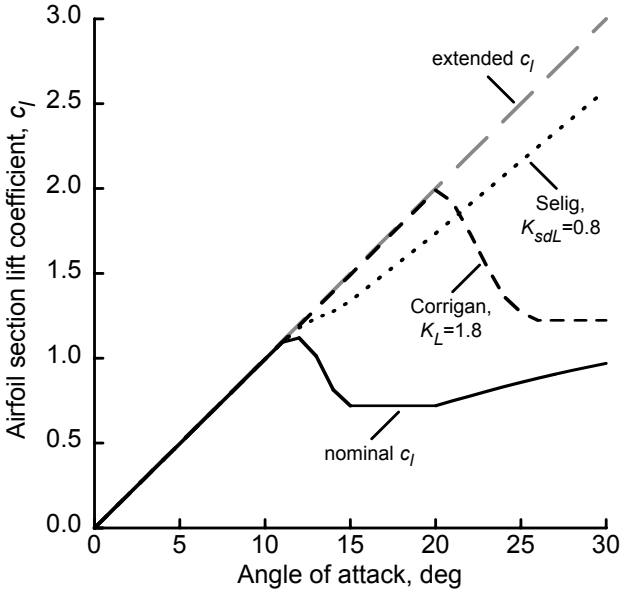

Figure 5. 3-D stall-delay models for the NACA 0012 airfoil compared with 2-D stall.

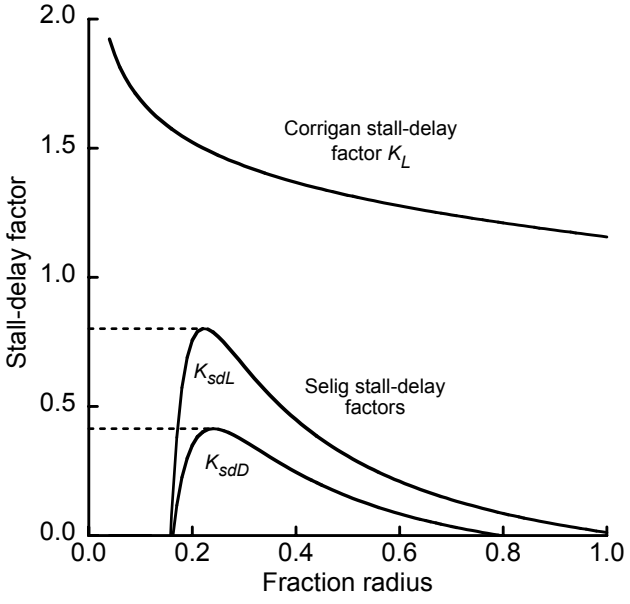

Figure 6. 3-D stall-delay factors vs. radius for the JVX planform.

The details of the stall-delay models are summarized as follows. For Corrigan stall delay, c_l is a function of α:

$$c_l = K_L c_{l\text{table}}\left(\frac{\alpha-\alpha_z}{K_L}+\alpha_z\right)$$

and K_L is a function of chord/radius:

$$K_L = \left(1.291(c/r)^{.0775}\right)^{1.8}$$

The singularity at the center of rotation is avoided by limiting the maximum value of K_L to that at $0.1R$. This stall-delay model is applied only to hover.

For Selig stall delay,

$$c_l = c_{l\text{table}} + K_{sdL}(c_{l_L} - c_{l\text{table}})$$
$$c_d = c_{d\text{table}} + K_{sdD}(c_{d_L} - c_{d\text{table}})$$

where

$$c_{l_L} = c_{l_\alpha}(\alpha-\alpha_z)$$
$$c_{d_L} = c_{dz}$$

The dependence upon chord/radius is given by

$$K_{sd} = \frac{1}{2\pi}\left[\frac{1.6c/r}{.1267}\frac{1-(c/r)^D}{1+(c/r)^D}-1\right]$$

where $D = R/r$ for lift and $D = R/2r$ for drag. This implementation of the Selig model is valid only for hover.

Reynolds Number Corrections

Reynolds number corrections to 2-D airfoils were developed in reference 16. The effect of Reynolds number on blade-section drag is modeled in CAMRAD II as

$$c_d = c_{d\text{table}}\left(\frac{Re_t}{Re}\right)^n$$

For the JVX predictions, $n = 1/5$ was used to model turbulent flow (ref. 16). Re_t was referenced to the wind tunnel test conditions at which the 2-D characteristics were measured for each blade airfoil section (ref. 6).

HOVER PREDICTIONS

Effect of Free-Wake Models

The CAMRAD II predictions of figure of merit (*FM*) are shown in figure 7 for the rolled-up and multiple-trailer wake models. The multiple-trailer model predicts JVX performance more accurately than the rolled-up model, particularly at low to moderate thrust.

The effect of the multiple-trailer wake on induced power is shown in figure 8, here plotted as the ratio κ of actual to ideal (momentum theory) induced power. The shift in the induced-power curve relative to the rolled-up model mirrors the shift in figure of merit (fig. 7).

Effect of Stall-Delay Models

Predictions made with the rolled-up model, but without stall-delay corrections, are shown in figure 7. Without stall delay, figure of merit is clearly underpredicted everywhere but at very low thrust.

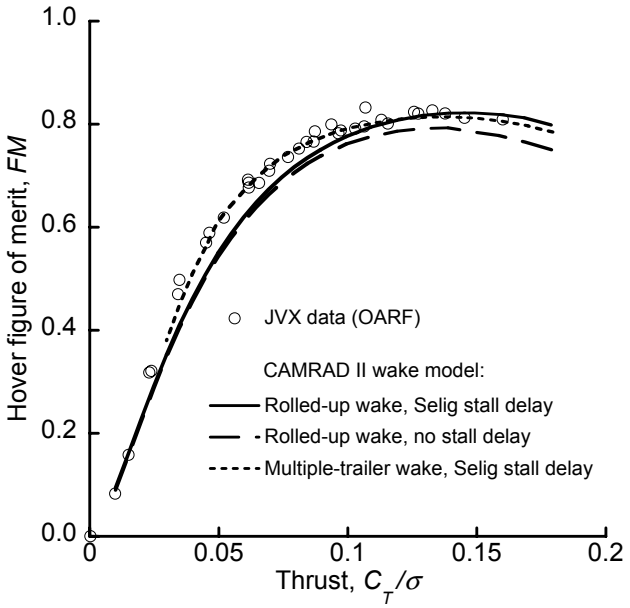

Figure 7. CAMRAD II predictions of JVX hover figure of merit compared with OARF test data. Predictions were made with the rolled-up wake model, with and without stall delay, and with the multiple-trailer wake model.

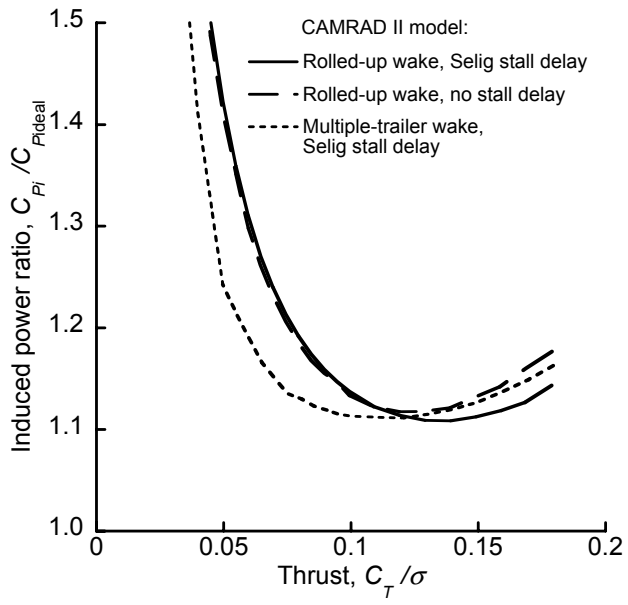

Figure 8. CAMRAD II JVX hover predictions of induced-power ratio for the rolled-up wake model, with and without stall delay, and for the multiple-trailer wake model.

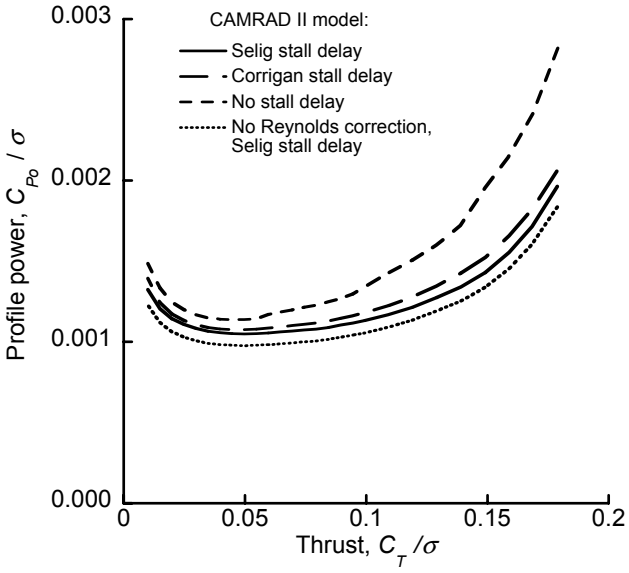

Figure 9. CAMRAD II hover predictions of JVX profile power for different stall-delay models and Reynolds number corrections, all with the rolled-up wake model.

At the scale of figure 7, predictions made with the Corrigan stall-delay model are nearly indistinguishable from those made with the Selig model and are therefore not included in the figure. To better illustrate the differences, profile power C_{Po}/σ is plotted in figure 9 for the two stall-delay models and with no stall delay. The difference between the two stall-delay models is clearly less than the effect of either alone compared to no stall delay. (Predicted C_{Po}/σ vs. thrust is almost identical for the rolled-up and multiple-trailer wake models, so the latter is not shown in fig. 9.)

Figure 8 shows the effect of the stall-delay model on predicted induced power. The Selig and Corrigan predictions are nearly identical, so only the former is shown in figure 8. Stall delay reduces the induced power only at high thrust.

Predictions made with the Selig and Corrigan stall-delay models differ only slightly, which is not surprising given that both models were empirically adjusted to match experimental data. The Selig model was used for all further predictions of JVX hover performance.

Effect of Reynolds Number Corrections

The effect of the CAMRAD II Reynolds number correction is of similar magnitude to the difference between the stall-delay corrections (fig. 9). The small effect of Reynolds number is to be expected, given the small difference in scale between the JVX rotor chord and the airfoils tested to develop the airfoil tables (ref. 6).

TRAM Hover Predictions

Figure 10 compares predictions using the rolled-up and multiple-trailer wake models with the TRAM 1/4-scale test data. The Selig stall-delay model was used for both sets of predictions. The improvement in predictions at low thrust can again be seen for the multiple-trailer model. Agreement is not as good as for the JVX rotor (fig. 7), probably because of the simplicity of the Reynolds number corrections (ref. 10).

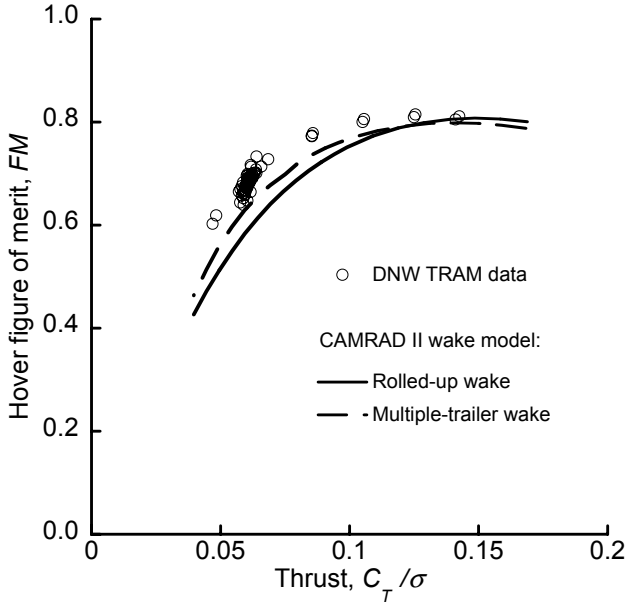

Figure 10. CAMRAD II TRAM predictions of hover figure of merit compared with DNW test data. Predictions were made with the rolled-up and multiple-trailer wake models.

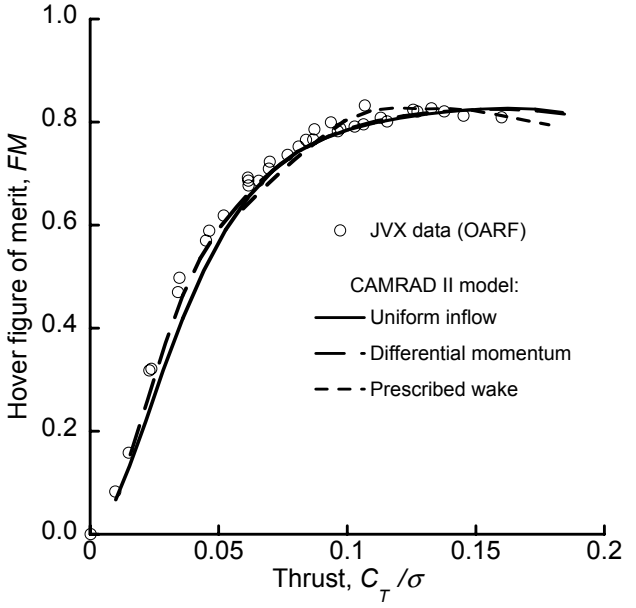

Figure 11. Comparison of CAMRAD II hover predictions for three simplified aerodynamic models with measured JVX figure of merit.

Additional Hover Models

Three additional, simpler aerodynamic models available in CAMRAD II were also investigated. In increasing order of sophistication, they were uniform inflow, differential momentum theory (the CAMRAD II implementation of combined blade-element/momentum theory), and the prescribed wake model of Kocurek and Tangler (ref. 17). Figure 11 suggests that they all match the test data better than the rolled-up free-wake model (fig. 7), but this conclusion is misleading. All three models in figure 11 rely upon empirical adjustments for good predictions of figure of merit. Figure 12 plots C_{Po}/σ for each model, revealing their differences more clearly.

Figure 13 shows predictions of the ratio κ of actual to ideal induced power for the three simpler models. The curve for uniform inflow would be flat if not for limited numerical precision at very low thrust. The differential-momentum predictions of induced power are in generally good agreement with the free-wake models (fig. 8).

The uniform inflow and differential momentum models use an empirical factor, κ_λ, multiplying induced velocity to obtain a good fit to *FM*. To match the JVX hover data,

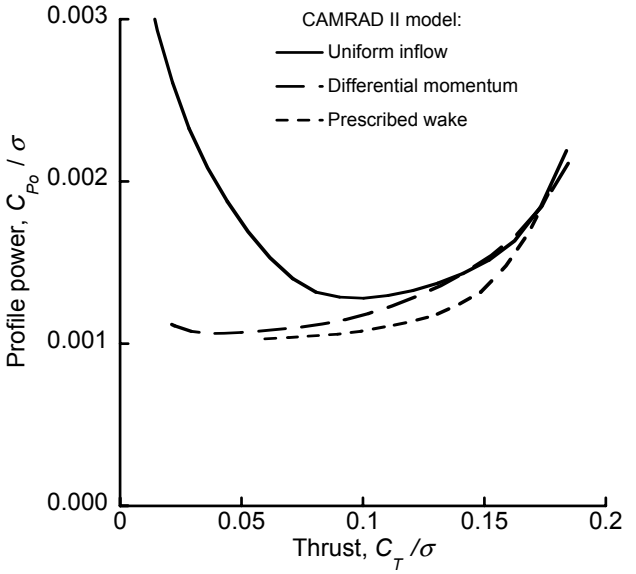

Figure 12. CAMRAD II hover predictions of JVX profile power for three simplified aerodynamic models.

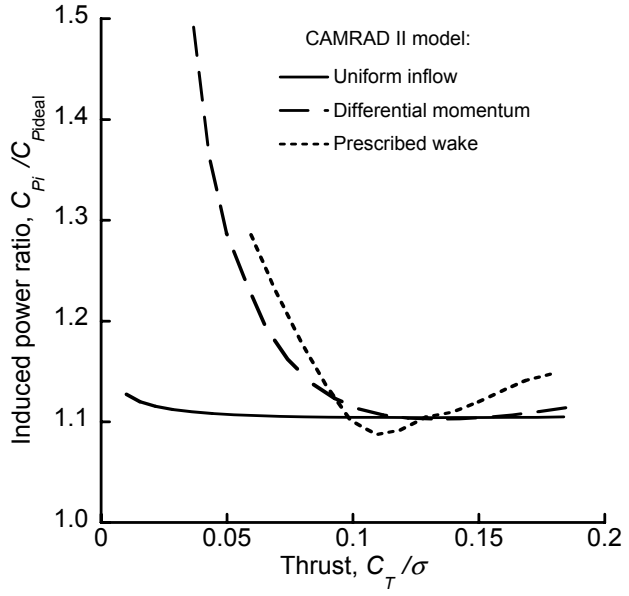

Figure 13. CAMRAD II JVX hover predictions of induced power ratio for three simplified aerodynamic models.

κ_λ = 1.10 for uniform inflow, and κ_λ = 1.04 for differential momentum. Because of the empiricism in choosing the appropriate values of κ_λ, these models cannot be relied upon to give good performance estimates as blade design parameters are varied. In addition, these two models do not account for the effects of wake distortion and vortex interactions. However, these simple models may be acceptable for high-speed axial flow, where wake effects on rotor performance are less important.

The Kocurek and Tangler prescribed wake model would seem to be a candidate for performance analysis, but this model also depends upon empirical adjustments, notably an adjustment of vertical convection. Moreover, the Kocurek and Tangler model estimates the vertical convection as a function of blade twist, number of blades, and C_T (equations are given in ref. 17). This model is based on helicopter twist rates, not the large twist rates of proprotors (and in fact is functionally invalid for large twist rates at low C_T). For the JVX rotor, the Kocurek and Tangler model is invalid below a C_T/σ of approximately 0.05. More advanced prescribed wake models are certainly possible, and the Kocurek and Tangler model could conceivably be modified to work better with the JVX rotor.

The CAMRAD II free-wake model is not free of empiricism; for example, the initial radial position of the tip vortex must be specified. Nevertheless, this model is not as dependent on the details of the blade design, in particular twist, as is the Kocurek and Tangler model. The free-wake model self-adjusts the wake geometry to match the particulars of the rotor configuration and operating condition, and does not rely upon empirical adjustments to induced velocity. Furthermore, CAMRAD II gains very little savings in computer time with a prescribed wake model, compared to the rolled-up free-wake model. For these reasons, prescribed wake models were not pursued further in the present study. However, an efficient prescribed wake model may prove useful for initialization of the free-wake geometry, so an opportunity exists for further development of prescribed wake models.

AIRPLANE-MODE PREDICTIONS

The JVX airplane-mode data are plotted as propulsive efficiency, η, versus thrust in figure 14. (Predictions are not shown in figure 14, so as not to obscure the data.) The data fall into a well-ordered pattern, but no single advance ratio, μ, has data that span the full range of thrust.

Measured JVX rotor power is plotted against thrust for a range of advance ratios in figure 15. Here, the ordering into five groups of constant μ is more evident and the CAMRAD II predictions can be easily compared to the data. All data at μ = 0.523 and below were taken at 487 rpm, but the data at μ = 0.562 were taken at 531 rpm. The CAMRAD II predictions in figure 15 are in good agreement with the experimental measurements.

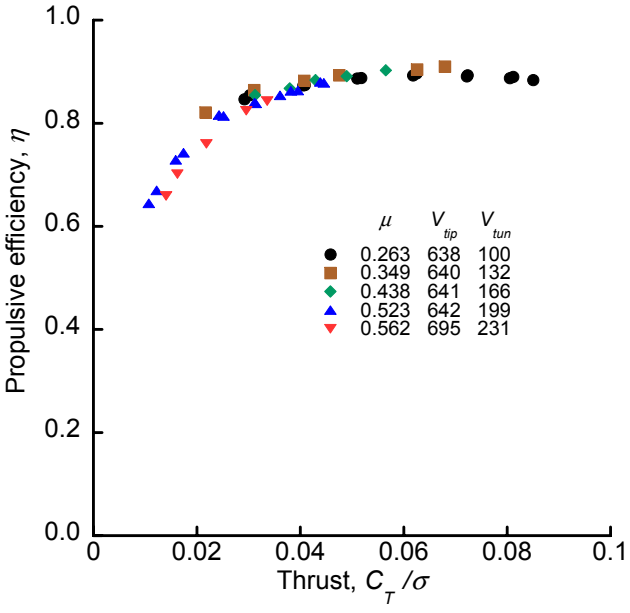

Figure 14. Measured JVX rotor propulsive efficiency from the NFAC Phase II test.

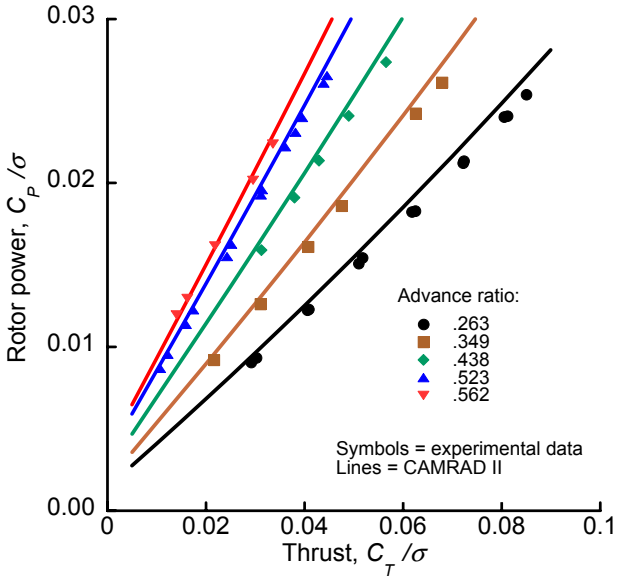

Figure 15. CAMRAD II predictions of JVX airplane-mode rotor power compared with test data for all advance ratios. The rolled-up wake model is used here.

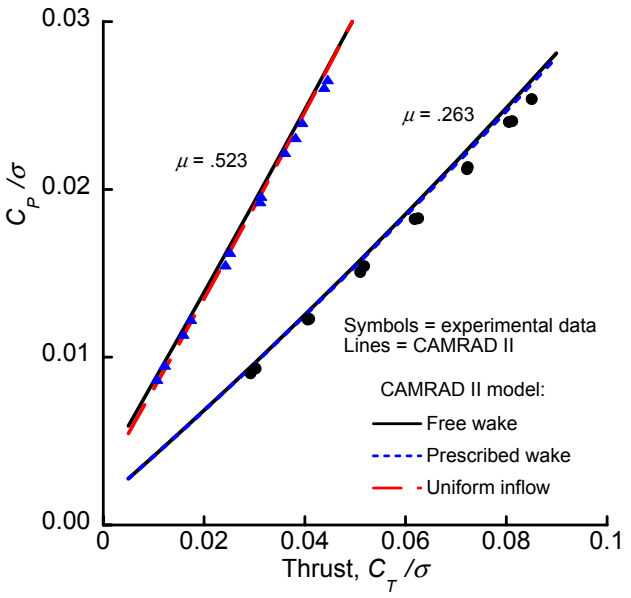

Figure 16. Predictions of JVX rotor power made with three different aerodynamic models compared with test data for two advance ratios.

The CAMRAD II predictions in figure 15 were made with the rolled-up free-wake model. Three-dimensional stall delay is not important at the low blade-lift coefficients typical of airplane mode at high speed, so no stall delay model was used.

The multiple-trailer model was not considered here, because blade-vortex interaction does not occur in high-speed axial flow, even at low thrust. There is, therefore, no advantage to be gained from higher-order wake models.

Airplane-mode performance predictions were made with three other CAMRAD II aerodynamic models: uniform inflow, differential momentum, and the Kocurek and Tangler prescribed-wake model (the same models used for hover predictions). All three were empirically adjusted for the best fit to the airplane-mode data as described for the hover predictions. The differences between all of these models for both η and C_P/σ are extremely small, usually less than one line thickness at the scale of figures 14 and 15.

Predictions with the greatest differences between models are shown in figures 16 and 17 for the two advance ratios with the most data points (μ = 0.263 and μ = 0.523).

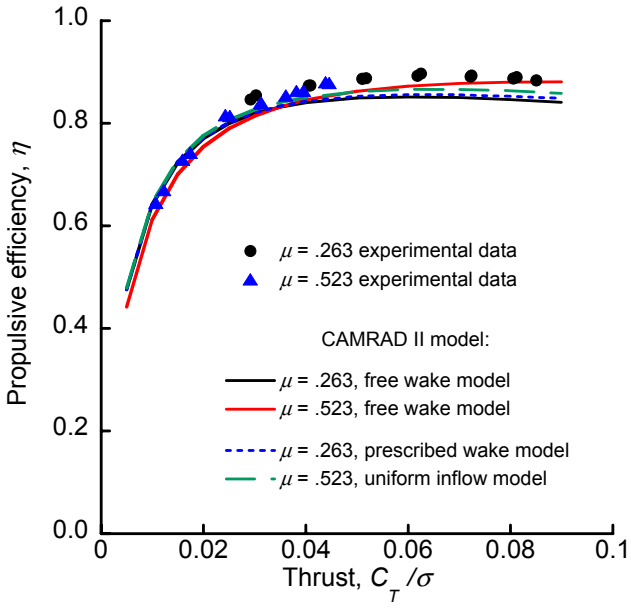

Figure 17. Predictions of JVX propulsive efficiency made with three different aerodynamic models compared with test data for two advance ratios.

Figure 16 plots power against thrust, and figure 17 plots propulsive efficiency against thrust. The former more clearly delineates the effect of advance ratio, whereas the latter is a more sensitive test of predictive accuracy. The Kocurek and Tangler prescribed-wake model differs slightly from the free-wake model at $\mu = 0.263$, and the uniform-inflow model differs noticeably from the free-wake model at $\mu = 0.523$, most evidently in figure 17. However, the discrepancy in the uniform-inflow model is greatest at combined high thrust and high μ, where no test data exist for comparison. Predictions made with differential momentum theory are always extremely close to the free-wake predictions, and are therefore not shown.

Although the CAMRAD II predictions using either the free-wake or differential-momentum models fit the data quite well, there remains a slight overprediction of power, particularly at low μ. The mismatch is not seen in predictions made for the TRAM model (figs. 18 and 19); at least, the mismatch is much smaller. The scales of figures 18 and 19 have been expanded relative to figures 15 through 17 for better legibility. However, the TRAM data extend over smaller ranges of thrust and advance ratio than do the JVX data, so definitive conclusions cannot be drawn from these comparisons.

Possible reasons for the mismatch between CAMRAD II predictions and JVX airplane-mode data may be summarized in four categories: blade modeling errors, limitations in the CAMRAD II wake model, deficiencies in the airfoil tables, and test data errors. The good fit to JVX hover data makes the first two possibilities unlikely, as does the good fit to TRAM airplane-mode data. The limited range of TRAM airplane-mode data leaves open a slight possibility of problems with the airfoil tables at high Mach numbers. Finally, known limitations of the JVX airplane-mode test data, discussed briefly as follows, make this a likely source of the problem, but this hypothesis has not been proved.

Reference 3 mentions concerns about JVX Phase I spinner tare corrections. Good spinner tare data are available only for the Phase I test, but the Phase II rotor data are more consistent than the Phase I data. The improved consistency and more comprehensive test conditions were motivations for examining only the Phase II data in detail. Because the Phase II test data may possibly contain residual tare errors, no significant effort was expended to improve the match between CAMRAD II performance predictions and JVX test data. There are no current plans for further testing to completely resolve the issue. Appendix A discusses JVX tare corrections in more detail. A discussion of TRAM tare corrections is given in reference 10.

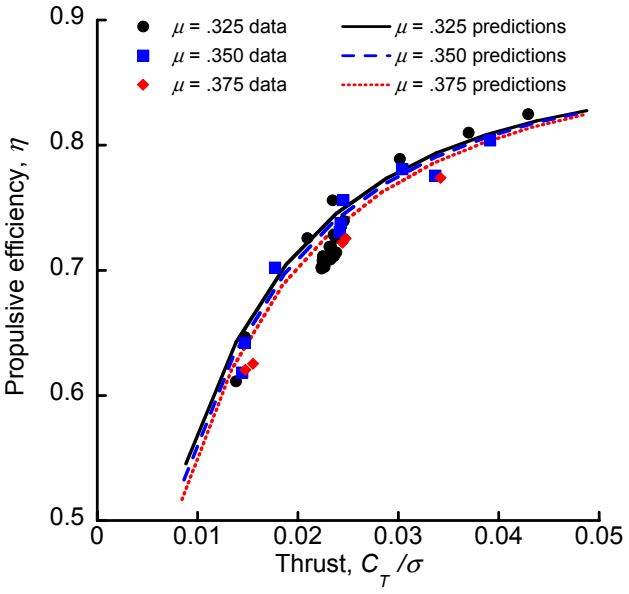

Figure 18. Predictions of TRAM propulsive efficiency made with the free-wake model compared with test data.

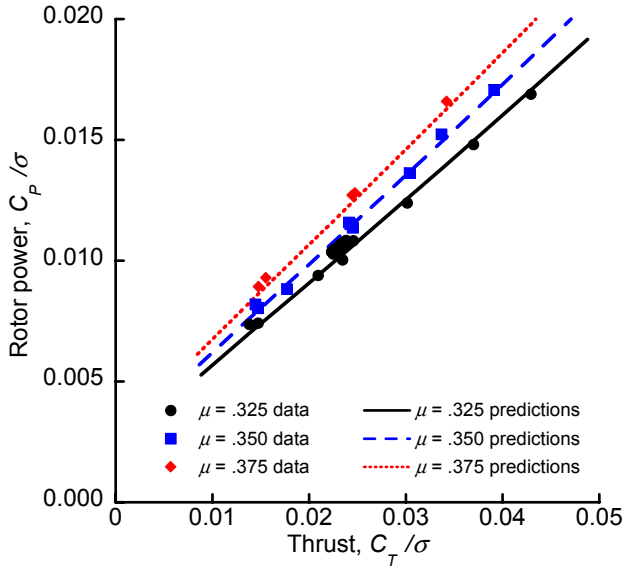

Figure 19. TRAM isolated rotor measured and predicted power (airplane mode). Predictions were made with the free-wake model.

CONCLUSIONS

Theoretical predictions of JVX proprotor performance were compared with experimental measurements for hover and airplane mode for an isolated rotor. Several different CAMRAD II aerodynamic models were evaluated to assess the appropriate level of sophistication required for rotor design optimization. The effects of Reynolds number corrections and two stall-delay models were also examined.

A free-wake model with a single tip vortex matched the hover data well at high thrust, but a multiple-trailer model was needed for accuracy at low thrust. However, the multiple-trailer model was much less efficient than the conventional model. Prescribed-wake (Kocurek and Tangler), differential-momentum, and uniform-inflow models could all be adjusted for a good fit to hover performance data, but the empiricism required to do so limits their suitability for design optimization.

Both the Corrigan and Selig stall-delay models provided equally goods fits to hover data. Reynolds number corrections had only a small effect on predicted performance, as was to be expected given the small difference in scale between the JVX rotor chord and the airfoils tested to develop the airfoil tables.

Equally good fits to airplane-mode data were achieved for differential-momentum, prescribed-wake, and free-wake models. A slightly degraded, but still reasonable, fit was achieved with uniform inflow. All but the free-wake model required adjustment of empirical constants to achieve the desired quality of fit.

For proprotor design studies, the conventional rolled-up free-wake model is recommended for hover predictions as the best compromise between accuracy and efficiency. For airplane mode predictions, the differential-momentum model is recommended because of its good accuracy and high efficiency. Occasional cross checks with the multiple-trailer model in hover and the rolled-up free-wake model in airplane mode may be in order to verify the accuracy of design optimizations.

REFERENCES

1. Johnson, W.; Yamauchi, G. K.; and Watts, M. E.: NASA Heavy Lift Rotorcraft Systems Investigation. NASA TP-2005-213467, Sept. 2005.

2. Felker, F. F.; Signor, D. B.; Young, L. A.; and Betzina, M. D.: Performance and Loads Data from a Hover Test of a 0.658-Scale V-22 Rotor and Wing. NASA TM-89419, Apr. 1987.

3. Felker, F. F.: Results from a Test of a 2/3-Scale V-22 Rotor and Wing in the 40- by 80-Foot Wind Tunnel. American Helicopter Society 47th Annual Forum, Phoenix, Ariz., May 1991.

4. Acree, C. W., Jr.: Calculation of JVX Proprotor Performance and Comparisons with Hover and High-Speed Test Data. American Helicopter Society Specialist's Conference on Aeromechanics, San Francisco, Calif., Jan. 2008.

5. Narramore, J. C.; Platz, D. A.; and Brand, A. G.: Application of Computational Fluid Dynamics to the Design of the BA 609. 25th European Rotorcraft Forum, Rome, Italy, Sept. 1999.

6. Jenks, M. D.; and Narramore, J. C.: Final Report for the 2-D Test of Model 901 Rotor and Wing Airfoils (BSWT 592). Bell-Boeing Report No. D901-99065-1, May 1984.

7. Rosenstein, H.; and Clark, R.: Aerodynamic Development of the V-22 Tilt Rotor. 12th European Rotorcraft Forum, Garmisch-Partenkirchen, Germany, Sept. 1986.

8. Young, L. A.; Booth, E. R.; Yamauchi, G. K.; Botha, G.; and Dawson, S.: Overview of the Testing of a Small-Scale Proprotor. American Helicopter Society 55th Annual Forum, Montréal, Canada, May 1999.

9. Potsdam, M. A.; and Strawn, R. C.: CFD Simulations of Tiltrotor Configurations in Hover. American Helicopter Society 58th Annual Forum, Montréal, Canada, June 2002.

10. Johnson, W.: Calculation of Tilt Rotor Aeroacoustic Model (TRAM DNW) Performance, Airloads, and Structural Loads. American Helicopter Society Aeromechanics Specialists' Meeting, Atlanta, Ga., Nov. 2000.

11. McCluer, M.: Tiltrotor Hover Performance Comparisons. Presented at the Naval Air Systems Command Air Vehicle Engineering Conference, La Jolla, Calif., May 2002.

12. Johnson, W.: Rotorcraft Aerodynamics Models for a Comprehensive Analysis. American Helicopter Society 54th Annual Forum, Washington, D.C., 1998.

13. Johnson, W.: Influence of Wake Models on Calculated Tiltrotor Aerodynamics. AHS Aerodynamics, Acoustics, and Test and Evaluation Technical Specialists Meeting, San Francisco, Calif., Jan. 2002.

14. Corrigan, J. J.; and Schillings, J. J.: Empirical Model for Stall Delay Due to Rotation. American Helicopter Society Aeromechanics Specialists Conference, San Francisco, Calif., Jan. 1994.

15. Du, Z.; and Selig, M. S.: A 3-D Stall-Delay Model for Horizontal Axis Wind Turbine Performance Prediction. AIAA Paper 98-0021, Jan. 1998.

16. Yamauchi, G. K.; and Johnson, W.: Trends of Reynolds Number Effects on Two-Dimensional Airfoil Characteristics for Helicopter Rotor Analyses. NASA TM-84363, Apr. 1983.

17. Kocurek, J. D.; and Tangler, J. L.: A Prescribed Wake Lifting Surface Hover Performance Analysis. American Helicopter Society 32nd Annual Forum, Washington, D.C., May 1976.

18. Advancement of Proprotor Technology, Task II—Wind-Tunnel Test Results. Bell Helicopter Company Report 300-099-004; also NASA CR-114363, Sept. 1971.

19. Acree, C. W., Jr.: A CAMRAD II Model of the V-22 Rotor for Whirl-Flutter Analysis. NASA TM–2004-212801, July 2004.

APPENDIX A: JVX TEST DATA

The JVX 1984 hover (ref. 2) and 1991 airplane-mode data used for this report are tabulated here. They generally include the highest-quality data that could be extracted from archives, but do not constitute the complete test dataset. The data presented in this report include all corrections identified in this appendix. Nevertheless, care should be taken when using the airplane-mode data, as is explained in detail in the relevant data section. Spinner drag tare data from the JVX 1988 airplane-mode test (ref. 3) are also included.

JVX HOVER DATA

The JVX hover data presented in the main body of this report are a subset of the data in reference 2 (Test 911). These test conditions are rotor only (no wing or ground plane), M_{tip} = 0.67–0.68, and ambient wind less than 1 knot. Table A1 lists the data meeting these criteria. V_{tip} is in ft/sec, wind speed in knots, and atmospheric density in slug/ft^3. C_T and figure of merit (*FM)* are corrected for ambient wind using the methodology described in reference 2.

For all comparisons between data and theory (CAMRAD II predictions) in the main body of this report, the values of V_{tip}, $M_{tip,}$ and ρ were averaged at each test condition, and ambient wind was assumed to be zero.

ERROR ANALYSIS

Insufficient data survive in the database to permit a fully rigorous error analysis. However, reference 2 states that the Propeller Test Rig (PTR) balance errors were within 0.3% of the maximum value of test for both thrust and torque. Taking these percentages as three times the standard errors of the balance calibrations, the standard deviation of *FM* for the JVX data can be estimated as 0.002. The exact value depends on the test condition; here the JVX hover design condition of C_T/σ = 0.15 was used. *FM* also depends upon ρ and V_{tip}. Including point-to-point data scatter of these two measurements increases the standard deviation of *FM* to 0.006.

The standard deviation of JVX η can similarly be estimated as 0.005, taken at C_T/σ = 0.045 at 199 knots. The propulsive efficiency η also depends upon V and V_{tip}, but almost all of the error is contributed by thrust. Adding data scatter in V and V_{tip} to the estimated error in η increases the standard deviation of η to 0.007.

It should be emphasized that these error estimates are not rigorous. However, they are sufficient to show that the errors (or scatter) in the measured data are less than the differences between the data and predictions shown in this report.

TABLE A1. JVX HOVER DATA (REF. 2); ROTOR ONLY; M_{tip} = 0.67–0.68; WIND LESS THAN 1 KNOT

Run	Point	V_{tip} (ft/sec)	M_{tip}	Wind (knots)	ρ (slug/ft^3)	C_T/σ	C_P/σ	FM
1	10	752.8	0.6768	0.81	0.002406	0.02311	0.002632	0.3183
1	11	752.8	0.6765	0.75	0.002404	0.03479	0.003107	0.4981
1	13	752.5	0.6762	0.64	0.002403	0.06134	0.005232	0.6926
2	6	759.4	0.6771	0.82	0.002363	0.00982	0.002789	0.0832
2	11	759.2	0.6761	0.87	0.002357	0.06159	0.005384	0.6771
2	14	758.9	0.6755	0.83	0.002354	0.08395	0.007577	0.7657
2	15	758.7	0.6753	-0.09	0.002354	0.09729	0.009185	0.7879
2	16	758.6	0.6752	0.13	0.002354	0.10291	0.009947	0.7916
2	17	760.6	0.6766	0.85	0.002351	0.11551	0.011682	0.8015
2	22	759.6	0.6760	-0.14	0.002354	0.16001	0.018856	0.8095
3	8	746.4	0.6747	0.62	0.002430	0.08109	0.007315	0.7529
3	9	746.3	0.6745	0.62	0.002430	0.09365	0.008545	0.7999
3	10	746.1	0.6743	0.98	0.002429	0.10685	0.010008	0.8324
3	11	749.5	0.6772	0.94	0.002428	0.11303	0.011202	0.8090
3	12	749.3	0.6769	0.90	0.002427	0.12562	0.012886	0.8240
3	13	749.2	0.6767	0.98	0.002426	0.13269	0.013941	0.8269
4	3	754.4	0.6774	0.84	0.002397	0.00024	0.003513	0.0003
4	4	754.4	0.6774	0.92	0.002397	0.01504	0.002777	0.1584
4	5	754.4	0.6773	0.64	0.002396	0.02382	0.002728	0.3213
4	6	754.3	0.6772	0.76	0.002396	0.03422	0.003209	0.4704
4	7	754.2	0.6771	0.92	0.002396	0.04635	0.004036	0.5896
4	8	754.1	0.6770	0.89	0.002396	0.06152	0.005300	0.6867
4	9	754.0	0.6768	0.95	0.002395	0.06986	0.006087	0.7234
4	11	753.8	0.6765	0.98	0.002394	0.08727	0.007819	0.7863
4	15	753.1	0.6756	0.54	0.002393	0.12731	0.013204	0.8205
4	16	752.9	0.6755	0.90	0.002393	0.13770	0.014849	0.8208
4	17	752.7	0.6751	0.99	0.002392	0.14523	0.016247	0.8124
6	6	755.6	0.6761	-0.05	0.002383	0.04507	0.004000	0.5704
6	7	755.5	0.6756	0.48	0.002308	0.05198	0.004569	0.6187
6	8	755.4	0.6753	0.47	0.002378	0.06558	0.005836	0.6863
6	9	755.4	0.6751	0.55	0.002377	0.06955	0.006163	0.7098
6	10	755.3	0.6749	0.42	0.002376	0.07684	0.006899	0.7364
6	11	755.2	0.6746	0.41	0.002375	0.08674	0.007949	0.7665
6	12	755.0	0.6745	0.13	0.002375	0.09636	0.009116	0.7825
6	13	754.9	0.6742	0.42	0.002373	0.10636	0.010391	0.7961
Averages:		754.1	0.6760	0.65	0.002389			

JVX AIRPLANE-MODE DATA

The JVX airplane-mode data were extracted from the Rotor Data Reduction System (RDRS) database (Test 579). Because of uncertainty in the measurement of rotor performance at very low wind tunnel speed, data below 30 knots are not included in this appendix. The data presented here are limited to five specific advance ratios. The objective is to prove a wide range of advance ratios with the constraint that each advance ratio includes data covering a reasonable range of thrust coefficients. A further requirement was that rotational speed be constant at a given tunnel speed, but this requirement eliminated only one data point.

Mean operating conditions and the C_T/σ range for each chosen advance ratio are listed in table A2.

TABLE A2. JVX MEAN CRUISE OPERATING CONDITIONS AND THRUST RANGES

μ	V_{tip} (ft/sec)	V_{tun} (knots)	C_T/σ
0.263	638	100	0.029–0.085
0.349	640	132	0.022–0.068
0.438	641	166	0.031–0.057
0.523	642	199	0.011–0.045
0.562	695	231	0.016–0.034

RDRS database label definitions and units are listed in table A3. The data are listed in tables A4 and A5 using the data labels in the database. Derivative data that can be readily recalculated, such as helical tip Mach number, are not included in the tables. In addition, spinner drag tare data from the 1988 Phase I test are listed in tables A6 and A7.

Spinner Drag Corrections

Reference 3 discusses the challenges of determining JVX spinner drag. The issues do not appear to have been resolved for the Phase II test. The spinner drag measurements from that test are unrealistic and were not used in the data analysis in the main body of this report. Spinner base pressures are stored in the RDRS database, but the spinner drag force (DSP, Table A3) is always zero. Therefore, the only available spinner drag correction is that derived from an assumed drag tare, adjusted by the base-pressure measurements.

It appears that the rotor drag data are mislabeled in the RDRS database, at least for the Phase II test. C_T/σ and η calculated from rotor drag without any spinner drag corrections are much more consistent than if calculated with a drag tare, with or without the base-pressure corrections. The XV-15 and JVX used the same hub and spinner, so their tares should be the same. The JVX Phase I mean spinner drag tare is 1.02 ft^2, which is consistent with an independently measured XV-15 spinner tare of 1.0 ft^2 (ref. 18). A drag tare error of 1.0 ft^2 would shift η by as much as 0.233, which is much larger than either the scatter in the data or the difference between the measured and predicted performance (e.g., see figs. 14 and 17). Closing the spindle holes in the spinner lowered the XV-15 spinner tare by about 0.1 ft^2 (ref. 18), which is not enough to explain the anomalies in the data.

For the Phase II data, the measured spinner base pressure is a nearly perfect fit to an area of 4.1 ft^2, which is a close match to the physical spinner base area of 3.9 ft^2. There was no evident speed dependency for the base pressure divided by tunnel dynamic pressure.

TABLE A3. JVX DATA LABELS, DEFINITIONS, AND UNITS

Label	Symbol(s)	Definition and units
COLL		rotor blade collective pitch, deg
CPS	C_P/σ	rotor power coefficient, divided by solidity
CTISS	C_T/σ	rotor thrust coefficient, divided by solidity
ETAIS,F	η	rotor propulsive efficiency
DSP		spinner drag, lb
MTUN		tunnel Mach number
PSI		yaw angle, deg
OMEG*R	$V_{tip} = \Omega R$	rotor tip speed, ft/sec
QPSF		corrected tunnel dynamic pressure, lb/ft^2
RHO100	ρ	tunnel air density, slug/ft^2
RPM		rotor rotational speed, rpm
RTRDFS		rotor drag force, including spinner loads, lb
SPBSF		spinner base force, positive in thrust direction, lb
TEMP		total tunnel temperature, deg F
TIPM		rotor tip Mach number
TORQC		corrected rotor shaft torque, ft-lb
VKTS	V_{tun}	tunnel air velocity, knots
V/OR	$\mu = V_{tip} / V_{tun}$	rotor advance ratio

Adjusting the uncorrected rotor drag with the spinner drag tare gave blatantly inconsistent results, as did all other attempts to back-calculate assumed corrections to the data. The conclusion is that the database is not in conformance with specifications, or at least the data are mislabeled. One conjecture is that RTRDFS in table A5 includes spinner tare and base pressure corrections, contrary to specifications. Unfortunately, not all intermediate calculations were stored in the database, so clear resolution of this issue is not possible. See the section "Phase I Tares" for further discussion.

The possibility remains that the wind tunnel data *with* spinner tare and back pressure corrections, exactly as given in the database, are accurate and include the effects of flow phenomena not modeled by CAMRAD II. Aerodynamic interactions between the spinner and the root of the blade, including the spindle and root airfoil section, are potential sources of error. Accordingly, spinner tare and back-pressure data are included in this appendix for comparison with other aerodynamic rotor models.

For all experimental data presented in this report, C_T/σ and η were based on the uncorrected rotor drag data (RTRDFS).

TABLE A4. JVX 1991 PHASE II AIRPLANE-MODE OPERATING CONDITIONS (TEST 579)

Run	Point	TEMP	RHO100	OMEG*R	VKTS	V/OR	TIPM	MTUN	RPM	QPSF
4	6	56.60	0.002332	637.8	99.5	0.2633	0.5739	0.1511	487.2	32.9
4	7	56.72	0.002331	638.7	99.6	0.2631	0.5746	0.1512	487.9	32.9
4	8	56.97	0.002330	635.8	99.7	0.2646	0.5719	0.1513	485.7	33.0
4	9	57.20	0.002329	639.8	99.5	0.2625	0.5754	0.1510	488.8	32.8
4	10	57.25	0.002329	641.8	99.6	0.2618	0.5771	0.1511	490.3	32.9
4	11	57.52	0.002327	638.5	100.2	0.2648	0.5740	0.1520	487.8	33.3
4	12	57.55	0.002327	640.9	100.2	0.2638	0.5762	0.1520	489.6	33.3
8	5	52.74	0.002355	635.5	98.7	0.2621	0.5739	0.1504	485.5	32.7
8	6	53.00	0.002354	636.8	99.1	0.2627	0.5750	0.1510	486.4	32.9
8	7	53.14	0.002353	638.0	99.1	0.2620	0.5760	0.1509	487.4	32.9
8	8	53.20	0.002352	635.9	99.2	0.2634	0.5740	0.1512	485.8	33.0
8	9	53.60	0.002350	638.3	99.5	0.2632	0.5760	0.1516	487.6	33.2
8	10	53.66	0.002350	636.7	99.5	0.2638	0.5745	0.1516	486.4	33.2
4	14	58.90	0.002304	639.1	131.8	0.3481	0.5747	0.2000	488.2	57.0
4	15	59.00	0.002303	636.6	132.2	0.3504	0.5725	0.2006	486.3	57.3
4	16	59.20	0.002302	640.9	132.3	0.3483	0.5762	0.2007	489.6	57.4
4	17	59.38	0.002301	638.9	132.2	0.3493	0.5743	0.2006	488.1	57.3
4	18	59.73	0.002299	640.9	133.0	0.3503	0.5759	0.2018	489.6	57.9
4	19	59.80	0.002298	641.8	133.0	0.3499	0.5767	0.2018	490.3	57.9
4	23	62.09	0.002265	642.5	165.8	0.4354	0.5774	0.2514	490.9	88.7
4	24	62.06	0.002266	639.8	165.6	0.4370	0.5749	0.2513	488.7	88.6
4	25	62.52	0.002263	637.9	166.2	0.4399	0.5730	0.2520	487.3	89.1
4	26	62.60	0.002263	639.4	166.2	0.4388	0.5744	0.2520	488.5	89.1
4	27	62.73	0.002264	643.1	166.7	0.4374	0.5776	0.2526	491.3	89.6
5	25	65.43	0.002234	642.5	199.2	0.5233	0.5771	0.3020	490.8	126.3
5	26	64.94	0.002237	643.1	199.1	0.5227	0.5779	0.3021	491.3	126.3
5	27	65.18	0.002235	639.0	199.3	0.5263	0.5741	0.3022	488.2	126.4
5	28	64.88	0.002236	642.8	199.8	0.5245	0.5777	0.3030	491.1	127.1
5	29	62.80	0.002246	638.5	198.9	0.5259	0.5750	0.3024	487.8	126.6
5	30	63.32	0.002244	640.2	198.7	0.5238	0.5762	0.3018	489.1	126.2
5	31	63.50	0.002243	641.6	199.1	0.5238	0.5773	0.3024	490.1	126.7
9	5	68.79	0.002237	641.4	198.8	0.5233	0.5742	0.3005	490.0	126.0
9	6	70.64	0.002229	643.6	198.8	0.5215	0.5751	0.2999	491.6	125.5
9	7	70.43	0.002230	643.9	198.9	0.5215	0.5755	0.3001	491.9	125.7
9	8	70.60	0.002230	644.7	198.4	0.5194	0.5761	0.2993	492.5	125.0
9	9	70.82	0.002229	644.3	199.5	0.5225	0.5758	0.3008	492.2	126.3
9	10	70.65	0.002230	642.3	199.4	0.5240	0.5741	0.3008	490.7	126.3
5	19	67.02	0.002197	695.5	231.3	0.5613	0.6257	0.3512	531.3	167.4
5	20	67.40	0.002195	695.7	231.1	0.5608	0.6257	0.3509	531.5	167.1
5	21	67.40	0.002196	693.0	231.0	0.5626	0.6233	0.3507	529.4	166.9
5	22	67.50	0.002195	694.5	231.4	0.5624	0.6246	0.3513	530.6	167.4
5	23	67.78	0.002193	696.2	231.7	0.5616	0.6260	0.3515	531.9	167.7

TABLE A5. JVX 1991 PHASE II ROTOR PERFORMANCE DATA (TEST 579)

Run	Point	RTRDFS	ETAIS,F	CTISS	COLL	TORQC	C_P/σ[1]	SPBSF
4	6	-1602.9	0.8546	0.03026	23.51	6173	0.00932	134.5
4	7	-2158.6	0.8736	0.04063	24.30	8126	0.01224	131.8
4	8	-2724.5	0.8881	0.05179	25.22	10148	0.01543	126.2
4	9	-3328.9	0.8970	0.06250	25.89	12176	0.01829	124.3
4	10	-3868.1	0.8910	0.07218	26.58	14208	0.02121	127.7
4	11	-4268.0	0.8876	0.08054	27.49	15916	0.02403	128.5
4	12	-4542.5	0.8840	0.08506	27.84	16945	0.02539	133.6
8	5	-1551.8	0.8467	0.02922	23.58	6005	0.00904	125.2
8	6	-2179.2	0.8742	0.04088	24.37	8186	0.01228	123.3
8	7	-2729.7	0.8869	0.05102	25.31	10081	0.01507	124.0
8	8	-3283.6	0.8927	0.06181	26.29	12110	0.01824	122.3
8	9	-3871.2	0.8930	0.07238	27.18	14264	0.02133	130.0
8	10	-4320.8	0.8900	0.08120	27.96	16010	0.02407	122.6
4	14	-1139.6	0.8210	0.02168	29.64	6039	0.00919	214.7
4	15	-1620.0	0.8644	0.03107	30.33	8209	0.01260	241.8
4	16	-2153.7	0.8824	0.04078	30.77	10627	0.01610	227.6
4	17	-2496.2	0.8932	0.04757	31.34	12202	0.01860	228.7
4	18	-3301.1	0.9042	0.06259	32.40	15986	0.02425	229.6
4	19	-3593.9	0.9100	0.06797	32.78	17273	0.02614	228.9
4	23	-1632.1	0.8547	0.03124	36.23	10393	0.01592	356.8
4	24	-1966.5	0.8679	0.03797	36.72	12378	0.01911	356.1
4	25	-2208.0	0.8836	0.04293	37.00	13739	0.02137	353.9
4	26	-2531.0	0.8914	0.04897	37.42	15575	0.02411	360.3
4	27	-2956.1	0.9029	0.05652	37.61	17900	0.02738	364.0
5	25	-630.3	0.6702	0.01224	40.87	6151	0.00955	510.7
5	26	-899.7	0.7427	0.01741	41.27	7915	0.01225	508.7
5	27	-1283.1	0.8144	0.02516	41.73	10365	0.01627	516.8
5	28	-1617.7	0.8384	0.03134	42.04	12651	0.01961	511.5
5	29	-1846.8	0.8544	0.03610	42.15	14209	0.02222	510.6
5	30	-2031.6	0.8634	0.03954	42.26	15407	0.02399	499.7
5	31	-2297.8	0.8787	0.04455	42.57	17123	0.02656	500.9
9	5	-550.7	0.6449	0.01072	40.62	5585	0.00869	500.6
9	6	-820.6	0.7293	0.01591	40.79	7334	0.01138	499.8
9	7	-1254.5	0.8160	0.02429	41.15	10021	0.01552	508.5
9	8	-1614.3	0.8399	0.03118	41.46	12479	0.01928	495.8
9	9	-1972.3	0.8630	0.03816	41.88	14928	0.02310	501.6
9	10	-2253.4	0.8805	0.04385	42.58	16761	0.02609	518.7
5	19	-834.4	0.6593	0.01406	44.04	8879	0.01197	676.2
5	20	-962.8	0.7017	0.01622	44.13	9618	0.01297	677.5
5	21	-1287.1	0.7602	0.02185	44.46	11907	0.01617	677.1
5	22	-1747.7	0.8243	0.02955	44.72	14905	0.02016	677.6
5	23	-1995.6	0.8432	0.03360	44.94	16614	0.02238	672.1

[1] C_P/σ is recalculated and does not match the database values of CPS, hence the change in label format.

TABLE A6. JVX 1988 PHASE I SPINNER TARE TEST CONDITIONS (TEST 568)

Run	Point	TEMP	RHO100	OMEG*R	VKTS	V/OR	TIPM	MTUN	RPM	QPSF
57	3	69.99	0.2271	649.3	131.2	0.3412	0.5777	0.1971	496	55.7
57	4	73.93	0.2253	648.0	131.4	0.3423	0.5744	0.1966	495	55.4
57	5	74.85	0.2250	648.0	131.2	0.3417	0.5739	0.1961	495	55.1
57	6	77.33	0.2220	648.0	165.3	0.4307	0.5738	0.2471	495	86.4
57	7	78.99	0.2213	648.0	165.2	0.4304	0.5729	0.2466	495	86.1
57	8	79.75	0.2210	648.0	165.1	0.4301	0.5725	0.2462	495	85.8
57	9	81.46	0.2177	648.0	203.0	0.5287	0.5734	0.3031	495	127.7
57	10	83.56	0.2169	648.0	203.0	0.5287	0.5722	0.3025	495	127.3
57	11	84.81	0.2165	648.0	202.9	0.5284	0.5716	0.3020	495	126.9
57	13	87.44	0.2140	648.0	220.7	0.5749	0.5711	0.3283	495	148.5
57	14	88.85	0.2135	648.0	220.5	0.5745	0.5703	0.3276	495	147.9
57	15	89.79	0.2132	648.0	220.4	0.5742	0.5698	0.3272	495	147.5
57	16	91.62	0.2109	649.3	238.4	0.6198	0.5710	0.3539	496	170.8
57	17	93.22	0.2105	648.0	238.2	0.6204	0.5690	0.3530	495	170.0
57	18	93.76	0.2102	649.3	238.1	0.6188	0.5699	0.3527	496	169.6

TABLE A7. JVX 1988 PHASE I SPINNER TARE DATA (TEST 568)

Run	Point	PSI	RTRDFS	DSP/QPSF
57	3	0	52.6	0.945
57	4	-3	61.2	1.104
57	5	-6	65.7	1.192
57	6	0	87.2	1.009
57	7	-3	92.2	1.071
57	8	-6	95.5	1.113
57	9	0	124.6	0.976
57	10	-3	127.6	1.003
57	11	-6	134.4	1.059
57	13	0	141.7	0.954
57	14	-3	145.6	0.985
57	15	-6	152.4	1.033
57	16	0	155.9	0.913
57	17	-3	161.4	0.949
57	18	-6	169.2	0.997
			Average:	1.020

Power Coefficient Calculations

The power coefficient C_P/σ (CPS) is calculated by the following equations in the database specifications:

CPS = CP / SIGMA

CP = TORQC / (DENOM * R)

DENOM = RHO * AREA * VTIP**2

where RHO is the air density and AREA is the total disk area.

For all data plots in this report, C_P/σ was recalculated from the rotor torque data (TORQC) using these formulas. The data stored in the database as CPS plot with severe scatter. The cause of the anomalies in the stored data was not determined.

Rotor shaft torque TORQC is corrected for shaft force interaction. Rotor drag force RTRDFS is the rotor balance axial force corrected for rotor shaft axial force and torque interactions. Tunnel dynamic pressure QPSF is corrected for compressibility.

Caution is advised when comparing these data with RDRS data from other tests. RHO100 usually means 100 times density, as in table A6, but the multiplication was evidently not applied to the JVX Phase II test data (table A4). DSP data were not stored for Phase II.

Phase I Tares

In the absence of reliable spinner drag measurements from the Phase II test, the best spinner tare data are those from the Phase I test. Test conditions and tare data are tabulated in tables A6 and A7, all at 495 to 496 revolutions per minute (rpm). Spinner base-pressure data were also stored for the Phase I test, but the values are an order of magnitude lower than those of Phase II and are therefore unrealistic.

APPENDIX B: THE CAMRAD II MODEL OF THE JVX TEST ROTOR

The following Fortran namelists are edited versions of the full CAMRAD II input files. Many inputs that use the CAMRAD II defaults have been deleted to reduce length, and many comments have been deleted or edited for clarity. Also, most of the inputs have been left in the default format. In CAMRAD II, namelist data override any previous data for the same parameters. This feature has been freely exploited for the Joint Vertical Experimental (JVX) model. The inputs are intended for use with CAMRAD II Release 4.6.

Job files are included for creating airfoil tables. Example hover and airplane-model jobs are also included. The job files are intended for use on an OpenVMS operating system and must be modified for the local system and directory structure.

MODEL INPUT DATA

Rotor Model

```
&NLDEF class='ROTOR',type='STRUCTURE',name='ROTOR 1',&END
&NLVAL
TITLE=' JVX OARF configuration -- NASA Version 7, Oct 2007',
! Version 7, 15 Oct 07: print gamma and Mach by default
RADIUS=12.5,NBLADE=3,ROTATE=1,SIGMA=.1138,  ! NASA TM-89419
   VTIPN=600.,
   GIMBAL=1,HINGE=0,
! Hub kinematics identical to XV-15:
   CONE=2.5,EPITCH=.091,KGMBL=25800.,       ! Bell XV-15 value
   CONTRL=2,PITCH=1,KPITCH=0.,LOCKP=1,
   XSP=.063,YSP=.017,ZSP= .088,             ! ref. zero pitch at .75 R,
   XPH=.059,YPH=.017,ZPH= .022,             ! simulate spider with
                                            !  overhead swashplate
   EPH=.11,LOCKPL=1,LOCKSP=0,KPL=22200.,
! Override shell swashplate stiffness (see also FLUTTER ROTOR):
   LOCKSP=1, KCOLL=1.E10,KLAT=1.E12,KLNG=1.E12,
   GDAMPU=.01,GDAMPV=.01,GDAMPW=.01,GDAMPT=.01,   ! blade analysis
   NINTEG=20,
   OPBEAM=2,DRELST=.04,KNODE=3,RNODE=.20,.40,.70, ! match XI,XC
   NSEN=2,QUANT=2*1,RLOAD=.05,.35,

NPROP=35,
RPROP=  0,0.05,0.051,0.06,0.061,0.087,0.0881,0.1,0.101,0.12,0.121,
        0.167,0.168,0.18,0.181,0.2,0.201,0.25,0.3,0.35,0.4,0.458,
        0.5,0.55,0.6,0.65,0.7,0.75,0.8,0.85,0.9,0.92,0.921,0.95,1.0,
THETAC= 14*27.47, 27.39,25.95,25.87,22.15,18.33,14.5,11.5,8.5,6.75,
        5,3.5,2,1,0,-1,-2.5,-4,-4.4,-4.42,-5.25,-6.75,
THETAI= 14*27.47, 27.39,25.95,25.87,22.15,18.33,14.5,11.5,8.5,6.75,
        5,3.5,2,1,0,-1,-2.5,-4,-4.4,-4.42,-5.25,-6.75,
TWISTA= 41.10,37.35,37.28,36.60,36.53,34.58,34.49,33.60,33.53,32.10,
        2.03,28.58,28.50,27.60,27.53,26.10,26.03,22.45,18.80,15.20,
        11.60,8.93,7.00,5.50,4.00,2.65,1.30,0.00,-1.30,-2.60,-3.90,
        -4.40,-4.43,-5.15,-6.40,
MASS=   1.3497,1.3497,1.218,1.218,1.218,1.218,1.307,1.307,1.23,
        1.23,1.23,1.23,1.23,1.23,1.23,0.302,0.302,0.302,0.253,
        0.216,0.183,0.162,0.149,0.142,0.13,0.124,0.12,0.117,0.111,
        0.105,0.1,0.1287,0.1287,0.1492,0.1362,


XI=  9*0.0,-0.00082,-0.00082,-0.0021,-0.0021,-0.00225,-0.00225,
     -0.00285,-0.00285,-0.00197,-0.0011,-0.00033,0.0,-0.00033,
     -0.00088,-0.00132,-0.00186,-0.00263,-0.00285,-0.0023,-0.00154,
     -0.00055,0.00055, 0.00114,0.00115,0.00175,0.00241,
```

```
XC=  9*0.0,-0.00082,-0.00082,-0.0021,-0.0021,-0.00225,-0.00225,
     -0.00285,-0.00285,-0.00197,-0.0011,-0.00033,0.0,-0.00033,
     -0.00088,-0.00132,-0.00186,-0.00263,-0.00285,-0.0023,-0.00154,
     -0.00055,0.00055, 0.00114,0.00115,0.00175,0.00241,
ZI=25*0.0, ZC=25*0.0,                                  ! no data

EIFLAP= 2*1944000,6*833000,2*1111000,1965000,1965000,2220000,2220000,
        2569000,1944000,1944000,1625000,1333000,1056000,781300,
        555600,375000,234000,28600,23100,18900,17700,39600,36200,31100,
        129000,120000,110000,101000,
EILAG=  2*1576000,6*833000,2*1111000,2340000,2340000,5556000,5556000,
        7174000,6150000,6150000,3472000,2847000,2548000,2347000,
        215000,2139000,2069000,1986000,1868000,1701000,1583000,1340000,
        1208000,1090000,1042000,1111000,1056000,958000,

! XV-15 pitch case ITHETA (approximate):
ITHETA= 0.0334,0.0285,0.0284,0.0275,0.0274,0.0248,0.0247,0.0236,
        0.0235,0.0216,0.0215,0.0170,0.0169,0.2737,0.3213,0.3104,
        0.0552,0.0433,0.0364,0.0317,0.0280,0.0251,0.0231,0.0211,
        0.0195,0.0178,0.0166,0.0154,0.0141,0.0128,0.0115,0.0114,
        0.0116,0.0105,0.0088,
! Assumed pitch case values, others = ITHETA:
IPOLAR= 13*0.0,0.2737,0.3213,0.3104,0.0552,0.0433,0.0364,0.0317,
        0.0280,0.0251,0.0231,0.0211,0.0195,0.0178,0.0166,0.0154,
        0.0141,0.0128,0.0115,0.01137,0.01157,0.01046,0.00881,
GJ=     4*88350,8*2569000,5*700000,625000,500000,406200,326400,259700,
        208300,163200,128500,100700,88000,55500,48900,42400,35900,
        33300,33300,29400,22800,

! EA, derived from EIs & KP:
EA= 3.20E+07,3.09E+07,3.09E+07,3.06E+07,3.06E+07,3.00E+07,3.00E+07,
    2.97E+07,2.97E+07,2.93E+07,2.93E+07,2.83E+07,2.82E+07,9.05E+07,
    5.83E+07,5.40E+07,6.09E+07,3.55E+07,2.91E+07,2.45E+07,2.04E+07,
    1.79E+07,1.63E+07,1.55E+07,1.34E+07,1.32E+07,1.24E+07,1.22E+07,
    1.09E+07,1.02E+07,9.70E+06,1.33E+07,1.37E+07,1.66E+07,1.64E+07,
XQC= -0.0161,-0.0150,-0.0150,-0.0148,-0.0148,-0.0142,-0.0142,
     -0.0139,-0.0139,-0.0135,-0.0135,-0.0125,-0.0125,-0.0122,
     -0.0122,-0.0118,-0.0118,-0.0107,-0.0097,-0.0086,-0.0076,
     -0.0063,-0.0054,-0.0044,-0.0033,-0.0023,-0.0012,-0.0001,
      0.0009, 0.0020, 0.0030, 0.0035, 0.0035, 0.0041, 0.0052,
ZQC= 0.0,                                              ! no data

! Assume elastic axis is same as 1/4 chord, outboard of pitch case:
XEA= 13*0.0, -0.0122,
     -0.0122,-0.0118,-0.0118,-0.0107,-0.0097,-0.0086,-0.0076,
     -0.0063,-0.0054,-0.0044,-0.0033,-0.0023,-0.0012,-0.0001,
      0.0009, 0.0020, 0.0030, 0.0035, 0.0035, 0.0041, 0.0052,
ZEA= 0.0,
```

```
! Assumed pitch case values:
KP= 0.0265,0.0270,0.0186,0.0187,0.0187,0.0188,0.0188,0.0189,
    0.0219,0.0220,0.0307,0.0312,0.0420,0.0235,0.0327,0.0310,
    0.0292,0.0303,0.0303,0.0307,0.0313,0.0315,0.0315,0.0308,
    0.0310,0.0303,0.0298,0.0290,0.0285,0.0279,0.0272,0.0238,
    0.0240,0.0212,0.0203,
KT= 0.0265,0.0270,0.0186,0.0187,0.0187,0.0188,0.0188,0.0189,
    0.0219,0.0220,0.0307,0.0312,0.0420,0.0235,0.0327,0.0310,
    0.0292,0.0303,0.0303,0.0307,0.0313,0.0315,0.0315,0.0308,
    0.0310,0.0303,0.0298,0.0290,0.0285,0.0279,0.0272,0.0238,
    0.0240,0.0212,0.0203,
&END
&NLDEF class='TRIM',&END
&NLVAL OPPART=2*3,                          ! need for GIMBAL=1
&END
!=====================================================================
&NLDEF class='ROTOR',type='AERODYNAMICS',name='ROTOR 1',&END
&NLVAL
! Min panel length=0.025, based on July 07 correlations
! 1st panel edge at 13.5 in, approx. inboard edge of raked cuff:
NPANEL=31,
REDGE=.09,.14,.19,.23,.27,.31,.35,.38,.41,.44,.47,
      .500,.525,.550,.575,.600,.625,.650,.675,.700,.725,
      .750,.775,.800,.825,.850,.875,.900,.925,.950,.975,1.,
NPROP=35,
RPROP= 0,0.05,0.051,0.06,0.061,0.087,0.0881,0.1,0.101,0.12,0.121,
       0.167,0.168,0.18,0.181,0.2,0.201,0.25,0.3,0.35,0.4,0.458,
       0.5,0.55,0.6,0.65,0.7,0.75,0.8,0.85,0.9,0.92,0.921,0.95,1.0,
CHORD= 2.038,2.002,2.001,1.995,1.994,1.975,1.975,1.966,1.965,1.952,
       1.951,1.918,1.917,1.908,1.908,1.894,1.893,1.858,1.822,1.785,
       1.749,1.707,1.677,1.641,1.605,1.569,1.533,1.496,1.460,1.424,
       1.388,1.374,1.373,1.352,1.316,

ASWEEP=35*1.91,                 ! result of structural sweep

NSEN=8,OPREF=7*4,               ! aerodynamic sensors:
QUANT= 5,25,53,54,35,75,82,82,  !   lambda
IDENT= 1, 0, 1, 1, 0, 0, 0, 0,  !   alpha,table alpha & Mach
AXIS=  3, 0, 0, 0, 0, 0, 1, 3,  !   theta, gamma
OPSCL= 2, 1, 1, 1, 1, 2, 2, 2,  !   Fx,Fz
NAPLOT=8*2,                     !  spanwise plots

! Bell (Corrigan) stall delay:
KLIFT=1.7490,1.7447,1.7446,1.7439,1.7437,1.7211,1.7181,1.6870,1.6845,
      1.6430,1.6409,1.5651,1.5637,1.5477,1.5465,1.5235,1.5224,1.4729,
      1.4320,1.3975,1.3678,1.3377,1.3181,1.2968,1.2772,1.2590,1.2421,
      1.2260,1.2109,1.1965,1.1828,1.1775,1.1772,1.1696,1.1569,
KLIFT= 100*1.0,      ! use Selig stall delay this version:
KSDL= 18*0.7706,0.6560,0.5435,0.4491,0.3605,0.3078,0.2546,0.2098,
      0.1717,0.1390,0.1105,0.0857,0.0639,0.0447,0.0376,0.0372,
      0275,0.0121,
KSDD= 18*0.4117,0.3664,0.3044,0.2459,0.1877,0.1520,0.1155,0.0845,
      0.0581,0.0354,0.0158,7*0.0000,
!  KSDL=100*0.0,KSDD=100*0.0,   ! airplane mode: no stall delay

OPREYN=1, ! Reynolds no. correction (drag only)
&END
!=====================================================================
&NLDEF class='ROTOR',type='INFLOW',name='ROTOR 1',&END
&NLVAL
    KHLMDA=1.10,KFLMDA=2.,FMLMDA=0., ! KHLMDA for uniform inflow hover
&END
!=====================================================================
```

```
! hover/propeller wake model
&NLDEF class='ROTOR',type='AERODYNAMICS',name='ROTOR 1',&END
&NLVAL MSPAN=0,NAPLOT=10*2,&END    ! output
&NLDEF class='ROTOR',type='WAKE',name='ROTOR 1',action='init',&END
&NLVAL
    OPSCEN=2,TWIST=-27.,RICWG=.26, ! hover wake, JVX
    FK2TWG=0.65,                   ! match to JVX hover
&END
&NLDEF class='ROTOR',type='WAKE',name='ROTOR 1',&END
&NLVAL OPSCEN=0,RNW=.25,WKMODL=8*2,
    OPFWG=3,                  ! general wake model
    OPDISP=0,0,               ! wake geometry sensor
    OPVOFF=0,                 ! no interference
    OPNW=0,                   ! 1st-order lifting line
    OPMCRC=0,0,               ! hover convergence
    OPRTV=1,RTVTX=.98,        ! tip vortex formation, 3 blades
&END
 !====================================================================
&NLDEF class='FLUTTER ROTOR',name='ROTOR 1',&END
&NLVAL
    OPMODE=1,DOFM=8*1,32*2,   ! blade modes
    DOFS=2,       ! need quasistatic swashplate to force high stiffness
&END
!====================================================================
&NLDEF action='end of shell',&END
&NLDEF action='end of core',&END
```

PTR Model (Generic Wind Tunnel Trim)

```
&NLDEF class='CASE',&END
&NLVAL
     TITLE='PTR (OARF)',
     CODE='HOVER PERFORMANCE',
     OPUNIT=1,OPDENS=3,DENSE=.002378,TEMP=59., ! environment
&END
!====================================================================
&NLDEF class='TRIM',&END
&NLVAL
     VELIN=1,WINDIN=1,VTIPIN=2,RPM=458.,
     LEVEL=1,                                   ! wake loop
     COLL=10.,CTTRIM=.08,MTRIM=3,               ! wind tunnel trim
     MNAME='CT/S    ','BETAS   ','BETAC   ',
     VNAME='COLL    ','LATCYC  ','LNGCYC  ',
     MHARMR=10,MHARMA=10,MHARMD=10,             ! part solution
     DOFA=6*0,DOFM=3*0,DOFD=8*0,
 &END
 &NLDEF class='TRIM ROTOR',name='ROTOR 1',&END
 &NLVAL OPMODE=0,DOFG=1,DOFB=12*1,&END          ! part solution
 !====================================================================
 &NLDEF class='FLUTTER',&END
 &NLVAL DOFA=6*0,DOFM=3*0,DOFD=8*0,&END
 &NLDEF class='FLUTTER ROTOR',name='ROTOR 1',&END
 &NLVAL
     OPWAKE=4,OPVATR=2,OPVRTA=2,                ! trim inflow
     OPMODE=1,DOFG=1,DOFM=4*1,36*2,DOFL=2,2*0,  ! degrees of freedom
     GDAMPM=40*.06,
 &END
 ====================================================================
 &NLDEF class='AIRFRAME',type='STRUCTURE',&END
 &NLVAL
     TITLE='PROPROTOR TEST RIG: JVX',
     CONFIG=0,OPFREE=0,                     ! wind tunnel
     OPAERO=0,                              ! no wing aerodynamics
     OPTRAN=0,                              ! no drive train
     MASSR=13.997,                          ! total rotor mass
     ASHAFT=-90.,                           ! PTR geometry
     HSP=2.,OPSPM=0,                        ! control system
 &END
 &NLDEF class='AIRFRAME',type='AERODYNAMICS',&END
 &NLVAL &END
 &NLDEF class='AIRFRAME',type='CONTROL',&END
 &NLVAL &END
 &NLDEF class='AIRFRAME',type='DRIVE TRAIN',&END
 &NLVAL &END
 ====================================================================
 &NLDEF class='TABLES',&END
 &NLVAL &END
 ====================================================================
 &NLDEF action='end of shell',&END
 &NLDEF action='end of core',&END
```

AIRFOIL TABLES

Inputs for airfoil tables (interpolated) follow. The C81 input tables are given in reference 19 and are derived from the wind tunnel data in reference 6.

```
$! JVX airfoil table creation job for OARF configuration
$! Requires V-22 tables with reference Reynolds no.
$ASSIGN [CAMRADII.V22]CLCDD959r.C81 INPUTDECK1
$ASSIGN [CAMRADII.V22]CLCDO957r.C81 INPUTDECK2
$ASSIGN [CAMRADII.V22]CLCDO956r.C81 INPUTDECK3
$ASSIGN [CAMRADII.V22]CLCDO955r.C81 INPUTDECK4
$ASSIGN [CAMRADII.JVX]JVX_OARF_af2.TAB OUTPUTTABLE
$DEFINE/USER_MODE SYS$OUTPUT [CAMRADII.JVX]JVX_OARF_af.OUT
$RUN CAMRAD2:INPUT
 BATCH
 &NLJOB OPFILE=7,OPSRC=1,&END
 &NLTABL OPFORM=2,RNTRP=0,
     TITLE='JVX ROTOR AIRFOILS (1 Sept. 98) OARF configuration',
     NRB=4,R=.225,.50,.75,1.0,
 &END

$! JVX airfoil table creation job for 40x80 configuration
$! Requires V-22 tables with reference Reynolds no.
$ASSIGN [CAMRADII.V22]CLCDET35r.C81 INPUTDECK1
$ASSIGN [CAMRADII.V22]CLCDD959r.C81 INPUTDECK2
$ASSIGN [CAMRADII.V22]CLCDO957r.C81 INPUTDECK3
$ASSIGN [CAMRADII.V22]CLCDO956r.C81 INPUTDECK4
$ASSIGN [CAMRADII.V22]CLCDO955r.C81 INPUTDECK5
$ASSIGN [CAMRADII.V22]V22af_r.TAB OUTPUTTABLE
$DEFINE/USER_MODE SYS$OUTPUT [CAMRADII.V22]V22af_r.OUT
$RUN CAMRAD2:INPUT
 BATCH
 &NLJOB OPFILE=7,OPSRC=1,&END
 &NLTABL OPFORM=2,RNTRP=0,
     TITLE='V-22 ROTOR AIRFOILS (1 Sept. 98) (ref. Re in tables)',
     NRB=5,R=.153,.254,.501,.751,1.0,
 &END
```

EXAMPLE JOB INPUTS

For convenience, inputs for all inflow models are given in the example jobs that follow. Normally, one would delete or comment out unused inputs. For example, the rolled-up wake jobs were run without the differential-momentum, prescribed-wake, or multiple-trailer inputs. The hover job includes the tight trim and circulation tolerances needed for good results at low thrust. The core inputs turn off calculation of the trim derivative matrix for computational efficiency. Only one trim case is given in each example job.

ITERP=0 skips the prescribed-wake iteration, as necessary for reliable trim at low thrust. It is inconsistent with LEVEL=2.

Hover Job with Multiple-Trailer Wake

```
$ SET VERIFY
$ ON WARNING THEN CONTINUE
$ ! JVX ISOLATED ROTOR
$ !
$ ! ** Hover performance (single rotor) of JVX
$ ! ** 397 rpm
$ !
$ASSIGN [CAMRADII.JVX]JVX_OARF_af.TAB           BLADEAIRFOIL1
$ASSIGN [CAMRADII.JVX]JVX_OARF.DAT              SHELLINPUT
$DEFINE/USER_MODE SYS$OUTPUT [CAMRADII.JVX]ct_mtw.out
$RUN CAMRAD2:CAMRADII
 &NLJOB NCASES=1, OPINIT=7, PLFILE=0, &END
 ========================================================================
 &NLDEF class='CASE',&END
 &NLVAL FLTASK=0,CODE='multi-trailer wake',
        OPDENS=1,ALTMSL=0.,
 &END
 &NLDEF class='TRIM',&END
 &NLVAL
  WINDIN=1,WKTS=0.,PITCH=0.,
  VTIPIN=3,RPM=397.,MTIP=.676,
  LEVEL=1,                    ! uniform inflow or differential momentum
  LEVEL=2,                    ! prescribed wake
  LEVEL=3, NWPRNT=0,          ! free wake
   MTRIM=1,TOLERT=1.,         ! wind tunnel trim
   MHARMR=0,MHARMA=0,MHARMD=0,
   MPSIAV=1,OPPART=1,         ! axisymmetric for hover (need GIMBAL=0)
   ITERF=7,RELAXF=.5,ITERP=0, ! wake convergence, skip prescribed wake
   TOLERC=0.10, RELAXC=0.5,0.1,2*0.05, ITERC=900,
   CTTRIM=.18,COLL=20.5,
 &END
 &NLDEF class='TRIM ROTOR',name='ROTOR 1', &END
 &NLVAL                      ! outputs:
     MHSEN=1,MCSEN=1,MBSEN=1,MASEN=1,MWSEN=1,MPSEN=1,
     MHTIME=1,MCTIME=1,MBTIME=1,MATIME=1,MPTIME=1,
 &END
 &NLDEF class='ROTOR',type='STRUCTURE',name='ROTOR 1',&END
 &NLVAL GIMBAL=0,&END                ! axisymmetric for hover
 &NLDEF class='AIRFRAME',type='STRUCTURE',&END
 &NLVAL CONFIG=0,OPAERO=0,OPTRAN=0,   ! no aerodynamics or drive train
        ASHAFT=0.0,                  ! no wind
 &END
 ========================================================================
 &NLDEF class='ROTOR',type='INFLOW',name='ROTOR 1',&END
 &NLVAL                      ! use differential momentum theory:
        OPDMT=1,             ! span differential
        OPTIP=1,             ! Prandtl tip loss correction
 &END
 &NLDEF class='ROTOR',type='INFLOW',name='ROTOR 1',&END
 &NLVAL KHLMDA=1.04,&END      ! match to differential momentum in hover
!========================================================================
 &NLDEF class='ROTOR',type='AERODYNAMICS',name='ROTOR 1',&END
 &NLVAL                      ! use multiple-trailer wake
```

```
        NTRAIL=2,TEDGE=0.80,  ! add trailer
        OPTRU=0,1,1,          ! not rolled up root
 &END
 &NLDEF class='ROTOR',type='WAKE',name='ROTOR 1',&END
 &NLVAL OPVCG=6,1, EXPVCG=2,2, RVCG=5,5,   ! square-law core growth
        ITERWG=8,                          ! wake geometry
 &END !=============================================================================
 &NLDEF action='end of shell',&END
 &NLDEF class='TRIM LOOP',type='NEWTON',name='TRIM',&END
 &NLVAL OPPID=0,DMTRX=.01,&END
 &NLDEF action='end of core',&END
$!#############################################################################
$!
```

Airplane-Mode Job with Rolled-up Wake; No Stall Delay

```
$! JVX cruise (airplane mode) performance
$!
$ SET VERIFY
$ ON WARNING THEN CONTINUE
$ASSIGN [CAMRADII.V22]V22AF_R.TAB                BLADEAIRFOIL1
$ASSIGN [CAMRADII.JVX]JVX_OARF.DAT               SHELLINPUT
$DEFINE/USER_MODE SYS$OUTPUT [CAMRADII.JVX]vr263.out
$R CAMRAD2:CAMRADII
 &NLJOB NCASES=1,OPINIT=7,&END
!=============================================================================
 &NLDEF class='CASE',&END
 &NLVAL
     CODE='no stall delay',
     OPDENS=3,DENSE=0.002340,TEMP=58.14,   ! Test 579 averages, by V/OR
 &END
 &NLDEF class='TRIM',&END
 &NLVAL
! equivalent to 0.75 MTIP (total) at 300 kts
  WINDIN=2,WVEL=.263,VTIPIN=2,RPM=487.,
  LEVEL=1,                    ! uniform inflow or differential momentum
  LEVEL=2,                    ! prescribed wake
  LEVEL=3, NWPRNT=0,          ! cruise free wake
   OPTRIM=1,MTRIM=1,TOLERT=.1,              ! trim
   MHARMR=0,MHARMA=0,MHARMD=0,MPSIAV=1,     ! axial flow
   MPSIAV=1,OPPART=1,         ! axisymmetric flow (need GIMBAL=0)
   ITERF=3,RELAXF=.5,         ! wake convergence
   TOLERC=0.05,ITERC=600,RELAXC=0.5,3*0.05,
   CTTRIM=0.005, COLL=22.0,
 &END
 &NLVAL                        ! outputs:
     MHSEN=1,MCSEN=1,MBSEN=1,MASEN=1,MWSEN=1,MPSEN=1,
     MHTIME=1,MCTIME=1,MBTIME=1,MATIME=1,MPTIME=1,
 &END
 &NLDEF class='ROTOR',type='STRUCTURE',name='ROTOR 1',&END
 &NLVAL GIMBAL=0,&END                  ! axisymmetric for hover
 &NLDEF class='AIRFRAME',type='STRUCTURE',&END
 &NLVAL CONFIG=0,OPAERO=0,OPTRAN=0,   ! no aerodynamics or drive train
 &END
```

```
!========================================================================
 &NLDEF class='ROTOR',type='WAKE',name='ROTOR 1',&END
 &NLVAL
     RFW=2.,MFWG=3,                                          ! cruise wake
 &END
!========================================================================
 &NLDEF class='ROTOR',type='INFLOW',name='ROTOR 1',&END
 &NLVAL                     ! use differential momentum theory
        OPDMT=1,            ! span differential
        OPTIP=1,            ! Prandtl tip loss correction
 &END
 &NLDEF class='ROTOR',type='INFLOW',name='ROTOR 1',&END
 &NLVAL KHLMDA=1.25,&END   ! match to differential momentum in cruise
!========================================================================
 &NLDEF class='ROTOR',type='WAKE',name='ROTOR 1',&END
 &NLVAL OPRWG=6,                                ! prescribed wake
        FK2TWG=0.67,                            ! match to JVX cruise
 &END
!========================================================================
 &NLDEF class='ROTOR',type='AERODYNAMICS',name='ROTOR 1',&END
 &NLVAL         ! root chord to match 40x80 test configuration:
  NPROP=35,
  RPROP= 0,0.05,0.051,0.06,0.061,0.087,0.0881,0.1,0.101,0.12,0.121,
         0.167,0.168,0.18,0.181,0.2,0.201,0.25,0.3,0.35,0.4,0.458,
         0.5,0.55,0.6,0.65,0.7,0.75,0.8,0.85,0.9,0.92,0.921,0.95,1.0,
  CHORD= 3*2.078, 14*2.137,                 ! cuff, extended to R=0
          1.858,1.822,1.785,1.749,1.707,1.677,1.641,1.605,1.569, 1.533,
          1.496,1.46, 1.424,1.388,1.374,1.373,1.352,1.316,
      KSDL =100*0.0,                        ! no stall delay for cruise
      KSDD =100*0.0,
      KLIFT=100*1.0,

      ASWEEP=17*0.0,18*1.91,                ! no sweep at cuff
 &END
!========================================================================
 &NLDEF action='end of shell',&END
 &NLDEF class='TRIM LOOP',type='NEWTON',name='TRIM',&END
 &NLVAL OPPID=0,DMTRX=0.02,&END
 &NLDEF action='end of core',&END
$!########################################################################
$!
```

REPORT DOCUMENTATION PAGE

Form Approved
OMB No. 0704-0188

1. REPORT DATE *(DD-MM-YYYY)*	2. REPORT TYPE	3. DATES COVERED *(From - To)*
27/04/2009	Technical Memorandum	

4. TITLE AND SUBTITLE
JVX Proprotor Performance Calculations and Comparisons with Hover and Airplane-Mode Test Data

5a. CONTRACT NUMBER

5b. GRANT NUMBER

5c. PROGRAM ELEMENT NUMBER

6. AUTHOR(S)
C. W. Acree, Jr.

5d. PROJECT NUMBER

5e. TASK NUMBER

5f. WORK UNIT NUMBER
WBS 877868.02.07.01.03.02

7. PERFORMING ORGANIZATION NAME(S) AND ADDRESS(ES)
Ames Research Center, Moffett Field, CA 94035-1000

8. PERFORMING ORGANIZATION REPORT NUMBER
A-090006

9. SPONSORING/MONITORING AGENCY NAME(S) AND ADDRESS(ES)
National Aeronautics and Space Administration
Washington, D. C. 20546-0001

10. SPONSORING/MONITOR'S ACRONYM(S)
NASA

11. SPONSORING/MONITORING REPORT NUMBER
NASA/TM–2009-215380

12. DISTRIBUTION/AVAILABILITY STATEMENT
Unclassified — Unlimited Distribution: Nonstandard
Subject Category: 01, 02, 05, 09
Availability: NASA CASI (301) 621-0390

13. SUPPLEMENTARY NOTES
Point of Contact: C. W. Acree, Jr., Ames Research Center, MS 243-12, Moffett Field, CA 94035-1000
(650) 604-5423

14. ABSTRACT
A 0.656-scale V-22 proprotor, the Joint Vertical Experimental (JVX) rotor, was tested at the NASA Ames Research Center in both hover and airplane-mode (high-speed axial flow) flight conditions, up to an advance ratio of 0.562 (231 knots). The hover and airplane-mode data were used to develop improved proprotor aerodynamic models. A new, multiple-trailer free-wake model is shown to give improved predictions of hover performance while also providing good predictions of airplane-mode performance. Predictions with simpler aerodynamic models are also included, along with discussions of stall-delay models and comparisons with Tilt Rotor Aeroacoustic Model (TRAM) hover data.

15. SUBJECT TERMS
Tilt rotor, Rotor aerodynamics, Rotor performance, Rotor testing

16. SECURITY CLASSIFICATION OF:			17. LIMITATION OF ABSTRACT	18. NUMBER OF PAGES	19a. NAME OF RESPONSIBLE PERSON
a. REPORT	b. ABSTRACT	c. THIS PAGE			C. W. Acree, Jr.
Unclassified	Unclassified	Unclassified	Unclassified	38	19b. TELEPHONE *(Include area code)* (650) 604-5423